Geophys. J. R. astr. Soc. (1984) 77, 883–914

Systematic analysis of deep seismicity: 200 centroid-moment tensor solutions for earthquakes between 1977 and 1980

Domenico Giardini *Department of Geological Sciences, Harvard University, Cambridge, MA 02138, USA and Dipartimento di Fisica, Settore Geofisica, Universita' di Bologna, Italy*

Received 1983 October 27; in original form 1983 June 5

Summary. A systematic study of deep seismicity is performed using waveform data from the GDSN between 1977 and 1980 and the Centroid Moment Tensor method of Dziewonski *et al.* Two hundred new CMT solutions are found for events deeper than 100 km; their moments, obtained using the same algorithm, range between 7×10^{23} and 1.4×10^{28} dyne cm – a factor of 20 000. A statistical analysis of the CMT parameters provides important conclusions. Among these, the shift in origin time for deep events is found to be almost independent of the seismic moment, providing an indication of the complexity of deep earthquakes. The deviation from the double couple model appears to be correlated to the state of stress of the subducting slabs; mechanisms showing down-dip compression are generally dominated by the eigenvalue corresponding to the compression axis, and down-dip tension correlates with the predominance of the tensional eigenvalue. Comparison with moment tensors obtained by other authors using different waveform data shows good agreement between different methods. Comparison with published focal plane mechanisms confirms the precision and reliability of the CMT method. Examples of CMT solutions used to identify patterns of seismicity associated with deep fault planes are shown.

Introduction

In recent years, the moment tensor representation of the seismic source has assumed a dominant role in modern seismology, owing to its capability of quantifying the size and geometry of earthquakes together with physical properties of the source.

Since 1977 the process of retrieving the moment tensor has undergone a major revolution with the introduction of the Global Digital Seismic Network (GDSN; see Peterson *et al.* 1976) and the International Deployment of Accelerometers (IDA; see Agnew *et al.* 1976). The availability of high quality digital data over a large dynamic range has made the moment tensor inversion a routine task.

Many methods have been proposed to retrieve the moment tensor from body waves, mantle waves and free oscillation data. Some are suitable, and currently used, for systematic

processing of large sets of events (Kanamori & Given 1981, 1982; Silver & Jordan 1982, 1983; Dziewonski, Chou & Woodhouse 1981; Dziewonski & Woodhouse 1983; Sipkin 1982).

The Centroid Moment Tensor method of Dziewonski *et al.* (1981) distinguishes itself by: (a) the combined use of body and mantle waves from the GDSN, extending the range of moments to values smaller than 10^{24} dyne cm, (b) the automatic inclusion in the inversion of all the body-waves phases, eliminating subjective decisions of the operator and assuring good depth control of the solution, and (c) the joint determination of the centroid and the moment tensor, allowing a better understanding of the source process. The CMT method is currently used in the systematic inversion of all the events with moment larger than 10^{24} dyne cm (Dziewonski & Woodhouse 1983; Dziewonski *et al.* 1983); this provides some 200–300 solutions every year, of which about 20 per cent are for intermediate depth and deep earthquakes.

The occurrence and the physical mechanism of deep earthquakes still remain a major problem in seismology. Seismic evidence from the observed distribution of first motions favours a mechanism dominated by shear failure, implying rupture on fault planes, although small volumetric components cannot be ruled out, and the contribution of phase changes to the faulting process is as yet unresolved. Moreover, the existence of patterns of seismicity that can be associated with planes of failure, as required by the double couple model, has been documented only for a very few cases (e.g. Fukao 1972; Billington & Isacks 1975; Billington, Isacks & Barazangi 1977), and the physical processes involved in the failure are still unknown.

In this study we apply the CMT method to an analysis of world-wide seismicity between 1977 and 1980, and we obtain a CMT solution for 200 intermediate depth and deep events; these represent more than one-half of all the moment tensor solutions for deep earthquakes available at the present time.

In the following sections we will briefly describe the theory and data used by the CMT method, present the results and the statistical properties of our solutions, and discuss in detail some particular events. We shall also report some results of a recent study which, making use of the CMT solutions, has established that deep events most often occur on identifiable fault planes, and finally apply our solutions to a survey of the state of stress in subducting slabs.

The CMT method

The Centroid Moment Tensor method of Dziewonski *et al.* (1981) consists of the inversion of waveform data for the simultaneous determination of the six independent components of the moment tensor and the coordinates of the centroid. The centroid is defined as the location in space and time which minimizes the first spatial and temporal moments of the stress glut distribution (Backus 1977). Essentially, the CMT inversion is an iterative procedure to locate the point source which best explains the observed seismograms.

The method is very general. For this study we use two sources of waveform data; specific long-period body waves from the GDSN (see Fig. 1), mainly from SRO and ASRO instruments, and surface waves from GDSN and IDA records.

The long-period body waves are low-pass filtered with a cut-off period of 45 s. The records are truncated before the arrival of fundamental mode surface waves, which are strongly affected by lateral heterogeneity at these frequencies; this procedure assures that all phases are automatically used in the inversion, including *p* and *s* surface reflections, essential in constraining the focal depth. The maximum spectral energy for these body waves ranges between periods of 50 and 70 s.

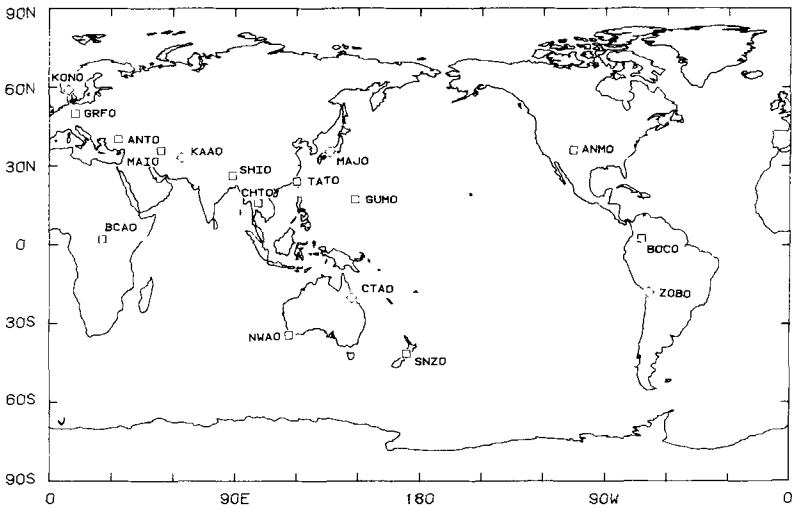

Figure 1. Distribution of SRO (indicated with □) and ASRO (▽) instruments of the GDSN. All stations operating at some stage between 1977 and 1980 are included.

The surface waves are filtered at a low-pass period of 135 s. Up to 4.5 hr of data are selected for each record after the response of the instrument becomes linear. The maximum spectral energy is for periods between 150 and 180 s.

Using mantle waves which travel along the major and minor arcs is very helpful because it doubles the effective azimuthal coverage. Also, for earthquakes with moments larger than 10^{27} dyne cm the body waves are seriously affected by source finiteness and complexity, and may become highly non-linear. Mantle waves allow the inversion for moments as large as 10^{28} dyne cm in this study, and the upper limit is probably close to 10^{29} dyne cm (hereinafter, moment tensor values will be understood to be expressed in dyne cm).

It is important to bear in mind that the CMT solution is obtained by fitting waveform data with synthetic seismograms. Some examples of the fit between data and synthetics are shown in Fig. 2(a–c). Of each pair of traces the upper one is the data and the lower is the synthetic seismogram obtained after the final inversion. The maximum amplitude, in equivalent SRO counts, is indicated. Examples of long-period body waves are shown in Fig. 2(a). Notice that the quality of the fit is as good for close stations as for distant stations (e.g. CHTO for the event of 1977 October 22), for which nearly 45 min of data are used. Fig. 2(b, c) shows examples of surface waves from IDA and GDSN stations. The delay is given in hours and indicates the starting time of the record, relative to the origin time of the event. Sometimes a few hours of data have to be omitted because of non-linearity; for example the data used for IDA station NNA begin more than 3.5 hr after the event.

The synthetic seismograms are obtained through summation of normal modes; with the cut-off period of 45 s used for long-period body waves, the number of normal modes is about 5000. The earth model PREM (Dziewonski & Anderson 1981) has been used for calculating periods and eigenfunctions of the normal modes, using the 'minor' method of Woodhouse (1981).

Because of the dataset used, two restrictions are imposed in the CMT method. First, since the waveforms are dominated by the shear energy the isotropic component of the moment tensor cannot be reliably detected. Thus, the linear constraint that the trace of the moment tensor must vanish is imposed: $M_{rr}+M_{\theta\theta}+M_{\phi\phi}=0$. Secondly, the energy of the long-period body waves is strongly concentrated in a range of periods from 50 to

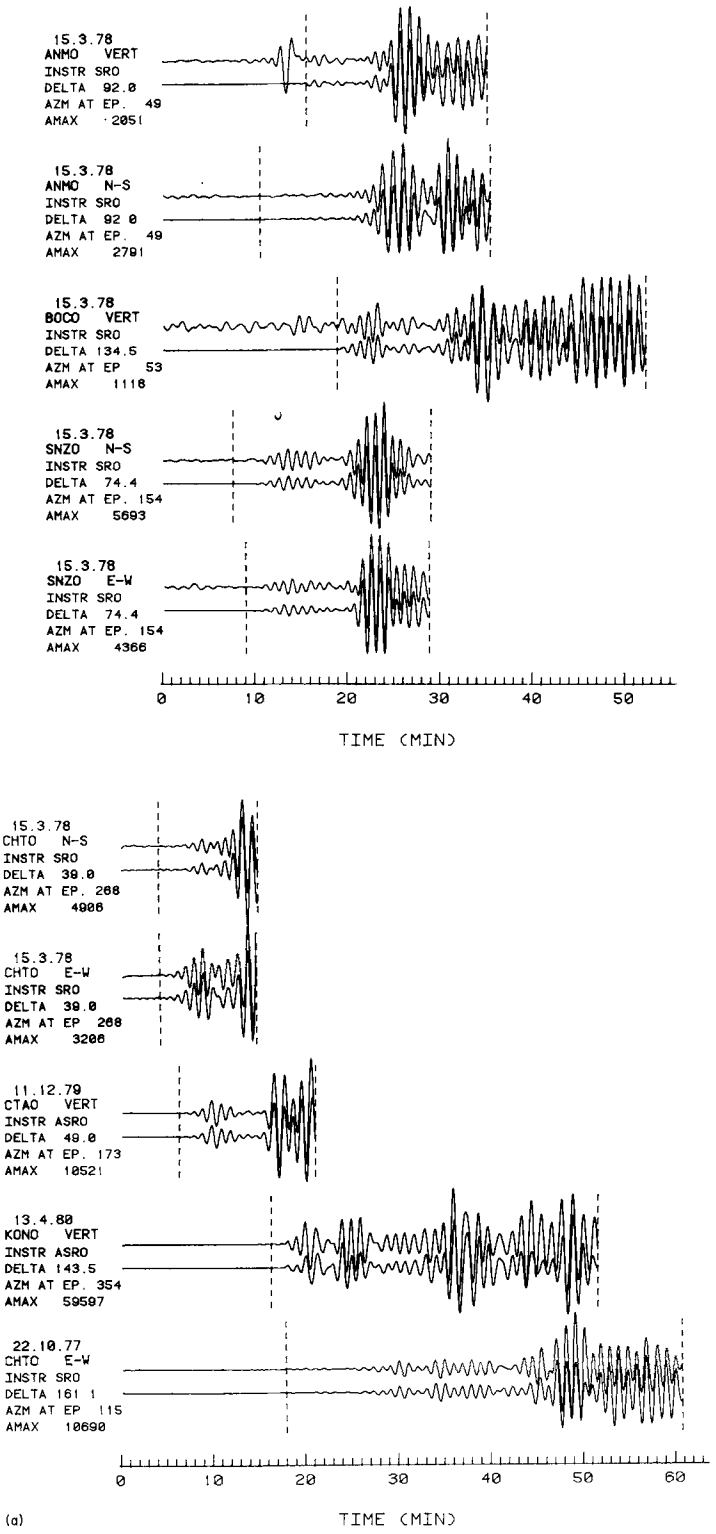

Figure 2(a)

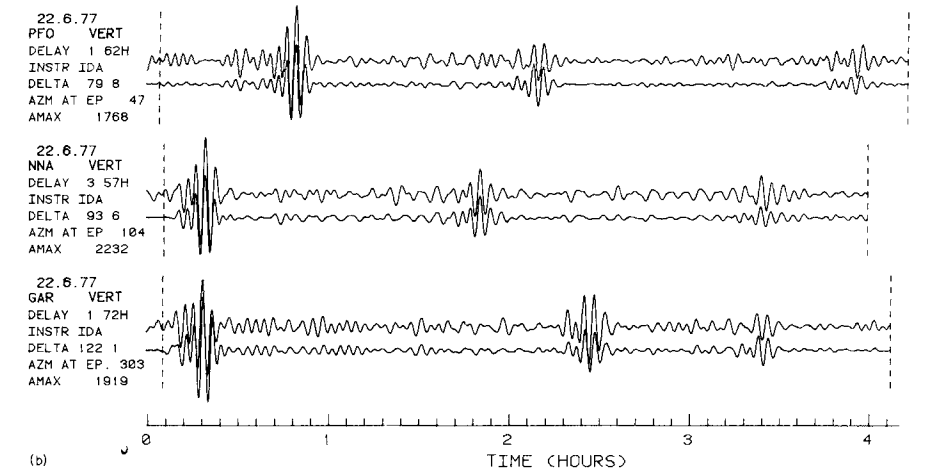

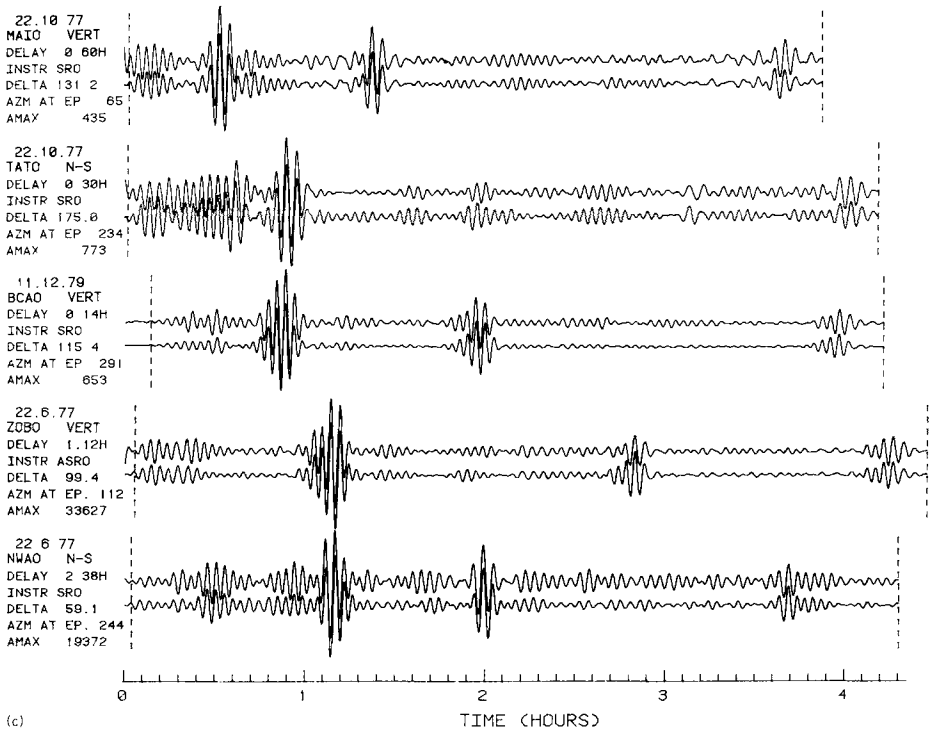

Figure 2. (a) Examples of comparison between waveform data (top record) and synthetic seismogram (bottom record) for body waves, low-pass filtered with a cut-off period of 45 s. For each trace the date of the event, the SRO/ASRO station, the type of instrument (vertical, north–south, east–west) and the geographical position of the station with respect to the epicentre (angular distance and azimuth) are indicated. The maximum amplitude of the trace is reported in digitial SRO count. Only data included between the dashed vertical lines are used in the inversion. The examples shown are for average (6.3×10^{25} dyne cm, 15/3/78) to large (2.8×10^{27} dyne cm, 13/4/80) size earthquakes and for depths of 125 (11/12/79), 166 (13/4/80), 270 (15/3/78) and 615 (22/10/77) km. (b) Comparison of waveform data and synthetic seismograms for mantle waves generated by the 22/6/77 event in Tonga Islands and recorded by the IDA stations NNA, PFO and GAR. A low-pass filter with a cut-off period of 135 s is used. The delay time represents the time elapsed from the origin time to the beginning of the record used in the inversion (expressed in hours). For further details see caption of (2a). (c) Examples of mantle waves recorded by GDSN instruments for the events shown in (a, b). See captions of (a and b) for explanations.

70 s. The spectrum of the moment rate tensor is therefore considered to be frequency-independent and, upon application of the appropriate correction, the CMT solution will correspond to the source spectrum at 0 frequency (see later section on the origin time).

Further details on the theory of the CMT method, the computations involved and the procedure used in analysing the data can be found in Dziewonski *et al.* (1981) and Dziewonski & Woodhouse (1983).

The data

The GDSN and IDA networks have been providing digital data of excellent quality since 1977. The SRO and ASRO instruments of the GDSN are characterized by a nominal dynamic range of 120 dB and allow us to recover moment tensor solutions for events with moments between 7×10^{23} and 1.4×10^{28} – a factor of 20 000 – using the same algorithm; the IDA instruments have lower dynamic range (66 dB), and are most useful in analysis of events with moments greater than 10^{26}.

At the beginning of 1977, when our analysis starts, the GDSN consisted of only six stations. This number of stations proves to be sufficient for the CMT inversion to converge in most cases. In this study IDA data have been included only for the 1977 June 22 event in Tonga; body waves are strongly affected by source complexity for events of this size and the dataset has to be increased to improve the azimuthal coverage and guarantee the reliability of the CMT solutions.

Towards the end of 1980 a few DWWSSN stations were added to the GDSN; the DWWSSN instruments have an average signal to noise ratio 10 times smaller than the SRO/ASRO, and can be used only for larger events.

Fig. 1 shows the distribution of the SRO and ASRO instruments which were active at some stage during 1977–80. Unfortunately some of these stations became inactive during this period and have not been replaced.

Results

The CMT method has been applied to all the events reported by the NEIS with body-wave magnitude $m_b \geqslant 5.5$ and depth $h > 100$ km. For some of these events it is impossible to obtain a solution. Some events are too small, even though they have magnitude larger than 5.5. Others occur within too close a time span of larger shallower earthquakes. Lastly, a few events happen close to midnight. The calibration pulse in GDSN records has a relatively large amplitude and, for moderate size earthquakes, records containing this pulse often have to be discarded.

A few events with m_b smaller than 5.5 have been analysed in regions of particular interest, like the Fiji Plateau region and southern Italy. Only some of these were found to have moments close to 10^{24}, the threshold for the CMT method. We also investigated a few very large events reported by the NEIS to have source depths shallower than 100 km, but which other investigations had located deeper.

Altogether we obtained 200 CMT solutions. Fig. 3 shows the geographical distribution of the events; all the subduction zones, characterized by intermediate depth or deep seismicity, are represented (in this paper, intermediate depth seismicity is meant between 100 and 300 km of depth). Fig. 4 shows the distribution of the logarithm of seismic moment as a function of centroid depth. The time period considered, 4 yr, is far too small to draw conclusions on cumulative moment release. Nonetheless, the curve is similar to plots of energy versus depth obtained by other authors for a much longer time period (e.g. Abe & Kanamori 1979).

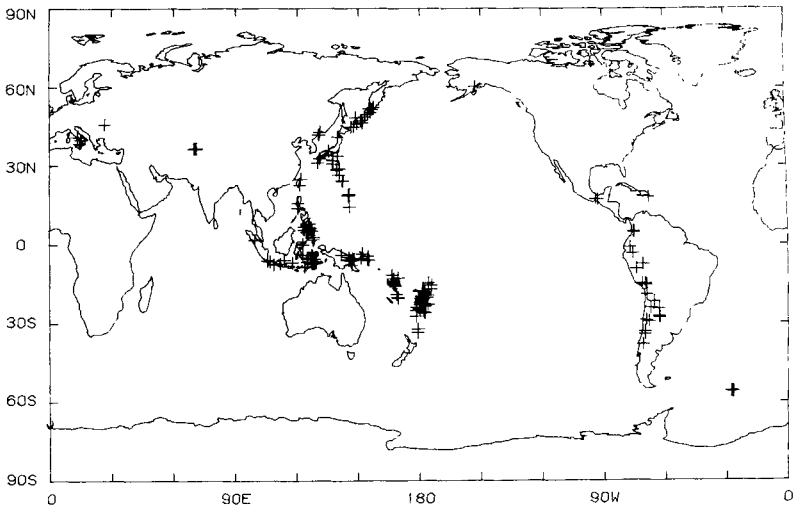

Figure 3. Distribution of the 200 events analysed with the CMT method. All the world-wide seismicity between 1977 and 1980, with $m_b \geq 5.5$ and deeper than 100 km, has been included in this study. All the subduction zones recognized to have intermediate depth or deep activity are represented.

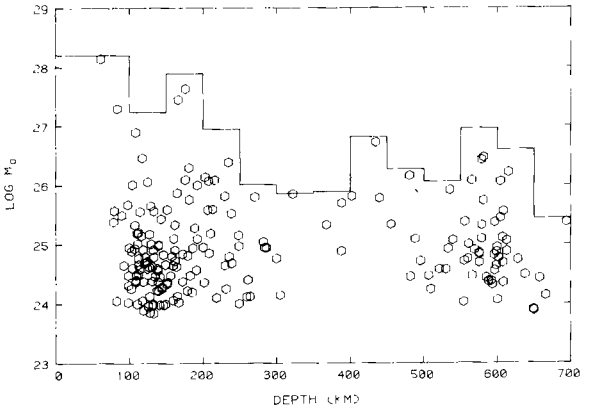

Figure 4. Plot of the logarithm of seismic moment versus CMT depth. The cumulative seismic moment released during the 4 yr period is also shown, calculated for 50 km depth intervals below 50 km.

The absence of any solution with moments smaller than 10^{25} at depths between 300 and 480 km could be related to the particular character of such intermediate depth events. Other studies, for example, have detected an increase in stress drop in the same range of depths (Chung & Kanamori 1980; Wyss & Molnar 1972).

The results for the 200 events are listed in Tables 1 and 2. Hypocentral position and origin time are those obtained with the CMT method; the perturbations are relative to the NEIS coordinates, published in *Monthly Listings*.

We compute the standard errors under the assumption that the errors are random and independent. As has been already pointed out (Dziewonski & Woodhouse 1983), this assumption is not entirely valid due to the lateral heterogeneity of the Earth, which is not taken into account in the PREM model. Systematic errors may also arise from discrepancies between the point source model and a real source distributed in space and time. In such cases, the formal standard errors may underestimate the real uncertainties.

Table 1. Centroid positions, shifts with respect to the hypocentres and origin times reported by the NEIS, and standard errors associated with the shifts for the 200 CMT solutions. The symbol '*' indicates events for which both body and mantle waves were used in the inversion. Also reported are the half-duration and the six components of the moment tensor solutions with the associated standard errors. The moment tensor components are scaled by a factor 10^{EX}.

NO.	DATE			TIME			*******		*** LATITUDE			***	*** LONGITUDE			***	*** DEPTH		****	HALF	EX	********** MOMENT TENSOR **********										**********			
	D	M	Y	H	M	SEC	DTO	SD	LAT	DLAT	SD		LONG	DLON	SD		H	DH	SD	DRTN		MRR		MTT		MFF		MRT		MRF		MTF	
																						VAL	SD	VAL	SD	VAL	SD	VAL	SD	VAL	SD	VAL	SD
1	1	1	77	17	35	54.9	0.0	0.2	-8.19	-0.30	0.04		108.82	-0.19	0.03		102.8	-10.2	2.6	3.0	24	-3.72	0.17	5.55	0.33	-1.83	0.28	5.82	0.18	-1.70	0.18	0.29	0.25
2	10	1	77	9	31	59.4	9.8	1.6	-20.75	-0.03	0.17		-179.70	-0.45	0.14		666.2	13.2	15.5	2.0	23	-2.30	1.41	8.90	1.83	-6.60	1.37	1.10	1.98	-9.93	1.52	-5.80	1.82
3	12	1	77	23	35	25.9	6.8	0.4	1.08	-0.50	0.04		99.50	-0.36	0.05		136.0	9.0	1.7	4.0	24	6.53	0.33	-6.76	0.45	0.23	0.48	0.04	0.31	-4.19	0.35	-3.79	0.49
4	21	1	77	6	11	11.8	6.2	0.5	-18.30	-0.29	0.05		-178.40	-0.02	0.04		607.0	1.0	2.9	3.0	24	-7.84	0.41	1.73	0.68	6.11	0.49	3.39	0.54	-9.82	0.53	-2.85	0.52
5	25	1	77	8	15	21.6	8.0	0.5	-16.17	-0.25	0.10		167.91	-0.32	0.06		260.8	-5.2	3.1	2.0	24	1.19	0.14	-1.14	0.25	-0.06	0.16	-0.33	0.14	-2.15	0.13	1.02	0.16
6	4	2	77	7	46	41.2	7.4	0.4	-25.05	-0.36	0.03		-62.91	0.45	0.07		565.1	16.1	2.1	3.0	26	-0.18	0.02	0.00	0.02	0.18	0.03	-0.56	0.03	1.04	0.03	0.11	0.02
7*	4	3	77	19	22	10.8	16.7	0.2	45.23	-0.54	0.03		26.17	-0.59	0.02		83.6	-10.4	1.1	17.0	27	1.78	0.04	-1.05	0.05	-0.73	0.03	-0.94	0.04	-0.59	0.02	-0.61	0.02
8	9	3	77	14	28	4.2	10.6	0.2	41.48	-0.13	0.02		131.55	0.57	0.03		578.6	50.6	1.6	4.0	26	1.14	0.04	-0.10	0.06	-1.04	0.07	-0.51	0.06	-2.21	0.06	-0.99	0.06
9	17	3	77	12	42	38.1	7.2	1.0	-12.92	-0.04	0.07		168.97	-0.41	0.08		649.0			3.0	23	-1.77	0.65	-5.23	0.70	6.99	0.49	4.72	0.83	1.78	0.78	1.01	0.88
10	22	3	77	2	23	20.0	2.2	0.4	-33.89	-0.29	0.08		178.81	-0.29	0.05		281.7	-54.3	2.3	2.5	25	0.13	0.04	0.08	0.07	-0.21	0.05	-0.28	0.04	1.05	0.04	-0.14	0.04
11	28	3	77	1	15	48.5	6.7	0.3	-15.16	-0.48	0.05		166.75	-0.35	0.03		111.9	2.9	2.1	3.0	25	0.51	0.04	-0.75	0.11	0.23	0.08	-0.83	0.04	-0.17	0.04	1.21	0.05
12	19	4	77	21	46	40.7	7.0	0.4	-5.62	-0.08	0.06		125.62	0.25	0.06		555.0	29.0	2.3	1.5	24	2.33	0.19	0.83	0.24	-3.16	0.25	0.74	0.25	-3.92	0.23	-1.76	0.25
13	20	4	77	20	4	35.4	6.0	0.3	30.34	-0.26	0.03		137.70	0.22	0.05		495.4	2.4	2.1	2.0	24	-4.11	0.14	2.57	0.21	1.54	0.25	-2.30	0.24	-0.39	0.20	2.85	0.21
14	22	4	77	23	11	53.2	5.3	1.1	-18.54	-0.79	0.13		-178.10	0.18	0.11		554.3	16.3	7.3	1.0	23	-6.00	0.82	6.74	1.40	-0.74	1.02	-2.76	1.02	-9.25	1.10	1.41	0.98
15*	13	5	77	11	13	36.7	5.5	0.2	28.12	-0.30	0.03		139.73	0.23	0.02		439.7	9.7	1.7	4.0	25	-3.29	0.10	0.81	0.14	2.48	0.12	1.12	0.11	-4.56	0.11	-2.58	0.12
16	15	5	77	23	13	0.7	7.1	0.7	-19.37	-0.24	0.07		-177.83	-0.16	0.05		506.4	7.4	3.3	2.0	24	-2.39	0.13	0.11	0.26	2.29	0.20	-0.19	0.20	-1.80	0.23	0.08	0.18
17*	21	5	77	5	35	30.9	8.4	0.2	15.39	-0.31	0.03		120.63	-0.19	0.03		189.4	-0.6	1.4	3.0	25	-0.43	0.04	1.22	0.06	-0.79	0.05	-1.01	0.04	-0.84	0.03	-0.90	0.04
18*	24	5	77	10	23	33.0	9.6	0.3	18.36	-0.45	0.03		145.51	0.16	0.02		206.1	-0.9	1.6	4.0	25	1.94	0.07	0.84	0.10	-2.79	0.09	-2.23	0.06	-0.42	0.06	1.89	0.08
19	31	5	77	14	48	3.9	4.8	0.5	-12.05	-0.24	0.04		166.03	-0.48	0.05		138.5	0.5	1.9	2.0	24	4.13	0.20	-1.23	0.25	-2.89	0.26	0.14	0.20	-0.30	0.20	0.79	0.25
20	3	6	77	2	31	7.8	3.1	0.4	36.06	-0.38	0.06		70.24	-0.52	0.04		210.0			3.0	24	9.34	0.52	-7.55	0.82	-1.79	0.66	8.67	0.40	-7.85	0.50	4.97	0.90
21	17	6	77	2	29	18.1	8.3	0.3	-19.86	0.02	0.03		-179.23	-0.13	0.03		693.9	3.9	2.7	3.0	25	-0.78	0.04	-0.09	0.05	0.87	0.05	-0.63	0.07	-1.47	0.06	-1.52	0.05
22	17	6	77	14	45	12.5	3.1	1.3	18.78	-0.26	0.11		145.39	-0.30	0.13		82.7	-25.3	9.3	2.0	24	-0.24	0.10	1.07	0.13	-0.83	0.18	-0.60	0.10	0.21	0.08	-0.28	0.15
23	19	6	77	11	47	32.7	9.3	0.4	46.38	-0.77	0.04		151.19	0.10	0.06		157.4	8.4	1.6	4.0	24	-1.43	0.23	-0.32	0.30	1.75	0.27	-3.75	0.22	-4.79	0.25	-2.44	0.27
24	19	6	77	7	32	20.2	6.4	0.3	4.80	0.15	0.03		125.41	0.48	0.03		283.5	12.5	1.6	2.5	24	-7.65	0.30	-1.07	0.42	8.72	0.41	-1.24	0.34	3.03	0.34	0.47	0.38
25-	22	6	77	12	9	22.1	48.7	0.3	-22.86	0.02	0.04		-174.91	0.99	0.03		61.3	-3.7	2.5	25.0	28	-0.49	0.02	-0.03	0.01	0.52	0.01	0.37	0.02	1.23	0.05	0.17	0.01
26	28	6	77	7	12	52.6	3.3	0.7	38.52	-0.11	0.12		14.39	-0.32	0.07		249.0	-12.0	3.9	1.5	23	-7.36	0.93	0.29	1.84	7.06	1.18	-7.66	0.77	0.70	1.00	2.34	1.12
27	6	7	77	11	28	39.7	8.2	0.3	-21.18	-0.11	0.04		-178.81	-0.24	0.02		596.2	2.2	1.8	3.0	25	-1.24	0.06	-0.81	0.10	2.05	0.07	-1.10	0.07	-1.04	0.08	-0.10	0.07
28	8	7	77	8	48	5.9	1.2	0.5	-6.06	-0.25	0.03		154.59	0.01	0.05		138.7	11.7	1.7	2.0	24	-2.06	0.11	1.57	0.13	0.50	0.17	-0.84	0.09	0.04	0.10	-1.18	0.14
29	10	7	77	1	42	42.5	6.0	0.3	-56.37	-0.25	0.03		-27.67	-0.11	0.05		116.7	-5.3	1.4	4.0	24	8.12	0.34	-4.21	0.53	-3.92	0.57	-6.79	0.29	-6.46	0.29	8.20	0.52
30	1	8	77	13	32	52.3	3.5	0.5	-20.61	-0.12	0.05		170.06	0.44	0.09		130.6	22.6	3.5	2.0	24	-1.70	0.19	0.08	0.31	1.62	0.29	2.77	0.20	2.46	0.17	1.23	0.25
31	4	8	77	1	11	17.3	6.2	0.3	-56.24	-0.23	0.03		-27.68	0.11	0.06		111.1	-0.9	1.8	3.0	24	6.15	0.28	-1.66	0.38	-4.48	0.49	-6.72	0.22	-2.82	0.21	5.24	0.46
32	10	9	77	13	39	7.7	6.0	0.3	-7.03	-0.46	0.04		106.90	-0.19	0.04		137.9	32.9	2.0	2.5	24	1.79	0.12	-0.76	0.15	-1.03	0.18	-2.70	0.11	-1.17	0.13	-2.27	0.16
33	21	9	77	21	1	51.8	7.8	0.3	51.04	-0.71	0.04		155.82	0.61	0.05		212.7	-18.3	1.2	3.0	25	-1.52	0.10	0.05	0.09	1.47	0.07	-2.92	0.09	-2.19	0.08	0.69	0.13
34	23	9	77	20	46	0.4	4.4	0.7	-5.42	0.34	0.06		129.18	0.35	0.10		394.8	-4.2	3.8	1.5	24	0.79	0.09	-0.33	0.11	-0.46	0.15	0.17	0.10	1.16	0.09	0.45	0.12
35	5	10	77	14	15	33.0	8.7	0.4	-18.66	-0.08	0.05		-177.92	-0.20	0.03		575.2	2.2	2.4	2.0	24	-4.69	0.20	2.16	0.32	2.53	0.23	-0.87	0.24	-3.18	0.25	0.22	0.23
36	8	10	77	3	3	58.3	6.8	0.6	-9.83	-0.31	0.06		-74.22	0.44	0.07		137.2	8.2	3.0	2.0	24	-1.26	0.10	-0.17	0.14	1.43	0.14	-0.46	0.09	-0.84	0.09	0.34	0.12
37	14	10	77	12	29	21.2	7.4	0.3	-15.68	-0.31	0.03		166.85	-0.56	0.02		123.6	-1.4	1.2	2.0	24	4.44	0.14	-0.05	0.28	-4.39	0.22	-2.15	0.14	-1.29	0.11	1.26	0.18
38	19	10	77	22	39	37.9	3.8	0.7	22.64	0.03	0.09		122.09	0.48	0.08		130.9	-27.1	2.8	2.0	24	-1.93	0.16	-0.56	0.21	2.49	0.19	0.60	0.14	0.75	0.12	0.17	0.20
39*	22	10	77	17	57	27.5	10.1	0.1	-28.13	-0.18	0.02		-62.62	0.35	0.02		614.9	0.9	1.0	5.0	26	0.55	0.02	-0.58	0.03	0.03	0.02	-0.75	0.02	1.47	0.02	-0.48	0.02
40	29	10	77	20	15	47.7	2.6	0.3	-6.45	-0.23	0.02		146.70	0.06	0.04		110.5	4.5	1.6	2.5	25	-0.46	0.04	1.15	0.06	-0.68	0.07	0.00	0.03	0.66	0.04	-0.96	0.05
41	30	10	77	6	25	36.9	6.9	0.6	-20.72	-0.30	0.05		-178.67	-0.10	0.06		595.4	-4.6	3.5	2.0	24	-2.20	0.17	2.46	0.23	-0.26	0.23	-4.85	0.29	-2.56	0.27	-3.11	0.21
42	30	10	77	12	53	27.1	4.3	0.4	-14.85	0.02	0.03		166.53	-0.42	0.04		106.8	3.8	2.2	3.0	25	0.08	0.04	0.93	0.09	-1.01	0.09	-1.00	0.05	-0.37	0.04	1.61	0.07
43	17	11	77	15	20	44.5	1.0	0.8	-56.31	-0.35	0.12		-27.80	0.06	0.21		127.4	0.4	6.1	2.0	24	1.23	0.14	-0.90	0.22	-0.33	0.20	-0.48	0.12	-0.67	0.14	0.32	0.21
44	17	11	77	17	20	33.6	1.0	0.7	33.64	0.00	0.06		140.40	0.53	0.07		103.6	-8.4	3.5	3.0	24	1.48	0.18	-1.37	0.28	-0.11	0.26	0.65	0.19	-2.58	0.17	-2.73	0.37
45	19	11	77	0	42	50.8	4.0	0.5	-56.15	-0.12	0.05		-27.69	0.14	0.09		134.4	-6.6	2.0	2.0	24	2.51	0.11	-1.94	0.17	-0.57	0.17	-0.06	0.10	-1.15	0.11	1.44	0.18
46	21	11	77	11	39	46.4	6.3	0.4	6.92	0.09	0.04		123.64	0.06	0.03		599.1	-1.9	2.5	2.0	24	-1.57	0.14	0.95	0.20	0.62	0.21	-2.99	0.24	-6.56	0.25	0.90	0.19
47	27	11	77	12	40	24.2	9.2	0.4	-20.68	-0.20	0.05		-178.49	-0.06	0.04		575.4	17.4	2.5	2.0	24	-1.55	0.18	2.03	0.29	-0.48	0.22	-5.34	0.24	-3.77	0.24	-0.53	0.19
48	30	11	77	10	15	51.8	8.4	0.4	-20.58	0.03	0.04		-178.62	-0.20	0.04		559.8	9.8	2.2	2.0	24	-3.03	0.13	2.54	0.21	0.49	0.20	-4.19	0.22	-2.57	0.23	-0.49	0.16
49	9	12	77	14	37	49.2	4.4	0.9	-6.86	0.32	0.09		130.26	0.92	0.10		146.0	5.0	2.9	1.0	24	1.01	0.08	-0.76	0.10	-0.25	0.12	0.27	0.08	0.26	0.08	-0.05	0.10
50	14	12	77	18	52	42.3	7.4	0.5	-21.01	0.09	0.05		-179.35	-0.20	0.04		657.6	-1.4	3.7	3.0	24	-1.36	0.11	-0.65	0.14	2.01	0.11	-1.47	0.12	-1.36	0.10	-0.04	0.09

Table 1 – *continued*

NO.	DATE			*******		TIME	*******	***	LATITUDE		***	***	LONGITUDE		***	***	DEPTH	****	HALF	EX	**********	MOMENT TENSOR	**********					
	D	M	Y	H	M	SEC	DTO	SD	LAT	DLAT	SD	LONG	DLON	SD	H	DH	SD	DRTN			MRR		MTT		MFF		MRF		MTF	
																					VAL	SD	VAL	SD	VAL	SD	VAL	SD	VAL	SD
101	11	12	78	3	33	59.6	6.8	0.3	-7.07	0.00	0.03	118.13	0.15	0.04	488.1	25.1	2.2	3.0	25	-1.23	0.04	1.04	0.05	0.19	0.06	0.46	0.06	-0.04	0.06	0.02	0.05
102	21	12	78	0	35	57.1	6.8	0.3	-21.98	-0.16	0.02	-179.45	0.05	0.03	612.8	19.8	2.1	3.0	24	0.98	0.12	-1.45	0.14	0.47	0.15	-3.61	0.17	-6.31	0.15	-1.35	0.11
103	27	12	78	17	46	14.7	4.3	0.3	41.11			13.58			387.7	-2.3	2.3	2.0	24	3.17	0.21	-1.72	0.37	-1.45	0.29	0.48	0.30	-4.98	0.31	-5.18	0.30
104	10	1	79	13	24	17.2	2.9	0.3	16.85	-0.09	0.03	-93.42	0.12	0.04	161.5	5.5	1.2	2.0	24	-0.01	0.18	-3.27	0.24	3.29	0.26	5.39	0.18	-4.92	0.20	-1.25	0.24
105	24	1	79	1	31	5.1	5.7	0.9	-6.16	0.08	0.08	155.54	0.31	0.11	148.7	-11.3	3.6	1.5	23	-5.79	0.65	2.87	0.88	2.92	1.01	-4.70	0.54	-2.71	0.67	-6.76	0.88
106	25	1	79	19	30	8.6	2.5	0.4	59.83	-0.30	0.03	-152.48	0.64	0.08	124.3	19.3	1.3	2.0	24	1.93	0.09	-3.60	0.15	1.67	0.13	0.02	0.08	2.19	0.09	0.94	0.14
107	29	1	79	5	43	10.4	9.6	0.6	-24.24	0.42	0.07	179.81	-0.15	0.06	509.4	6.4	3.3	1.5	24	-0.55	0.07	-0.02	0.11	0.57	0.10	0.19	0.10	-1.64	0.09	0.00	0.10
108	31	1	79	12	36	28.6	4.0	0.3	42.92	0.14	0.03	130.95	-0.25	0.03	575.2	30.2	2.7	2.0	24	1.82	0.20	0.28	0.17	-2.10	0.18	0.98	0.21	-4.60	0.22	-4.98	0.20
109	7	2	79	21	2	9.5	2.7	0.2	5.13	-0.08	0.03	127.29	-0.01	0.03	128.7	-0.3	1.2	4.0	25	4.20	0.13	-1.08	0.17	-3.13	0.18	-0.57	0.11	-2.05	0.10	-1.24	0.19
110	9	2	79	2	0	13.7	1.4	0.3	-56.35	-0.03	0.05	-27.00	-0.11	0.08	102.6	-1.4	3.8	1.5	24	1.01	0.08	-0.32	0.13	-0.69	0.14	-1.27	0.07	0.92	0.07	0.28	0.12
111	11	2	79	22	22	24.9	4.0	0.2	6.13	0.14	0.04	126.24	0.32	0.04	142.5	0.5	1.0	3.0	25	2.05	0.07	0.02	0.09	-2.08	0.08	-1.09	0.07	0.88	0.06	-1.07	0.09
112	14	2	79	16	55	11.4	7.5	0.3	-15.87	-0.31	0.03	167.17	-0.40	0.04	126.8	3.8	1.6	3.0	25	1.10	0.04	0.30	0.06	-1.40	0.06	0.05	0.04	-0.82	0.04	-0.05	0.05
113	27	2	79	4	1	31.4	2.6	0.6	-14.95	0.02	0.04	166.98	-0.35	0.06	109.3	-0.7	3.3	2.0	24	0.18	0.08	-1.44	0.17	1.26	0.15	-0.56	0.09	0.47	0.08	-1.77	0.14
114	6	3	79	3	46	28.8	3.7	0.6	-5.66	0.20	0.03	145.35	-0.44	0.09	110.3	3.3	2.6	2.0	24	-0.65	0.05	1.17	0.08	-0.51	0.11	-0.09	0.04	-0.12	0.07	-0.34	0.07
115	29	3	79	1	11	39.4	7.4	0.3	-24.09	-0.04	0.03	178.19	-0.36	0.03	568.6	24.6	1.7	2.0	24	-3.49	0.14	0.66	0.21	2.84	0.19	0.02	0.21	6.93	0.19	-2.14	0.19
116	30	3	79	17	10	27.3	1.5	0.8	-56.15	0.02	0.08	-27.26	-0.01	0.14	125.6	-6.4	4.4	2.0	23	4.30	0.66	3.36	1.02	-7.66	1.03	-5.98	0.63	-0.98	0.62	2.86	1.02
117	15	4	79	22	14	57.3	4.9	0.2	5.56	-0.12	0.02	123.66	0.04	0.02	535.6	-13.4	1.4	4.0	25	-4.20	0.11	3.09	0.15	1.11	0.14	0.68	0.16	-6.47	0.17	-3.52	0.13
118	17	4	79	4	22	2.3	6.1	1.3	-6.55	0.43	0.09	129.92	0.23	0.15	132.5	7.5	5.0	1.5	23	1.82	0.61	-2.28	0.84	0.45	0.98	-0.64	0.52	1.15	0.53	6.68	0.80
119	24	4	79	1	45	16.6	7.6	0.2	-20.81	0.02	0.03	-178.90	-0.21	0.02	604.2	5.2	1.6	3.0	25	-2.16	0.05	1.37	0.06	0.79	0.06	-1.97	0.07	-0.51	0.07	0.46	0.06
120	23	4	79	11	39	34.6	-2.1	1.0	2.27	0.41	0.11	128.45	0.18	0.10	141.0	13.0	8.0	2.0	23	1.59	1.02	-1.63	1.57	0.04	1.66	9.37	1.08	1.07	1.06	0.36	1.47
121	7	5	79	12	52	8.9	2.6	0.2	-6.41	-0.10	0.03	105.67	-0.29	0.03	118.4	1.4	1.8	2.0	24	0.98	0.13	3.58	0.24	-4.56	0.27	2.38	0.13	-3.80	0.16	-5.43	0.28
122	13	5	79	6	26	12.5	4.7	0.2	18.79	-0.21	0.02	145.42	0.08	0.02	215.6	-35.4	1.2	4.5	25	6.47	0.22	0.93	0.34	-7.39	0.38	-6.62	0.22	-2.72	0.23	7.36	0.34
123	13	5	79	17	31	1.4	4.6	0.2	-4.09	-0.04	0.02	122.96	-0.19	0.03	613.0	-2.0	1.7	2.5	25	0.05	0.02	-0.37	0.02	0.32	0.02	0.34	0.03	-1.04	0.02	0.13	0.02
124	14	5	79	15	40	0.4	7.4	0.4	44.43	-0.33	0.05	147.05	-0.54	0.05	108.5	0.5	2.4	2.0	24	1.23	0.09	1.22	0.17	-2.44	0.14	0.56	0.08	-1.41	0.09	0.90	0.11
125	18	5	79	20	18	7.9	6.8	0.2	23.94	-0.19	0.02	142.66	0.26	0.03	580.9	13.9	1.8	3.0	25	-5.64	0.15	3.97	0.18	1.67	0.20	-0.22	0.23	-0.36	0.23	2.23	0.18
126	21	5	79	22	22	36.6	13.0	0.2	-15.70	-0.45	0.03	-69.70	0.39	0.02	234.0	26.0	1.3	5.0	26	0.04	0.04	0.13	0.07	-0.17	0.07	2.37	0.05	-0.36	0.05	0.61	0.06
127	25	5	79	18	15	44.1	3.1	0.3	24.01	-0.10	0.03	142.08	-0.16	0.05	578.7	-12.3	2.4	2.0	24	-6.65	0.32	6.07	0.49	0.57	0.45	-8.70	0.50	6.33	0.50	1.40	0.48
128	12	6	79	23	11	3.0	0.3	0.2	-55.97	0.01	0.03	-28.39	-0.52	0.05	111.7	-20.3	2.0	3.0	24	-0.18	0.08	0.88	0.15	-0.70	0.16	-3.06	0.08	0.50	0.08	-0.25	0.13
129	19	6	79	17	30	25.4	4.6	0.3	-14.77	-0.26	0.03	166.88	-0.34	0.03	112.0	-10.0	2.2	3.0	24	-2.74	0.12	2.33	0.22	0.42	0.20	-3.57	0.13	-0.17	0.11	1.37	0.18
130*	22	6	79	6	31	5.1	10.8	0.2	17.65	0.65	0.02	-93.97	0.64	0.02	117.1	10.1	1.1	7.0	26	-1.89	0.04	-0.47	0.04	2.36	0.04	1.56	0.03	-0.12	0.04	-1.19	0.04
131*	25	6	79	5	29	13.9	8.3	0.2	-4.91	0.07	0.01	145.50	-0.08	0.02	192.1	3.1	0.9	5.0	25	-9.49	0.15	6.17	0.18	3.32	0.22	4.69	0.14	-0.87	0.14	-3.28	0.14
132	26	6	79	3	4	56.1	4.3	1.0	35.11	-1.37	0.13	72.19	0.97	0.11	263.9	34.9	5.4	2.0	24	-1.16	0.12	1.28	0.18	-0.12	0.13	-0.52	0.12	0.09	0.16	-0.18	0.16
133	27	6	79	21	46	30.1	4.7	0.3	-29.58	-0.10	0.03	-68.56	-0.28	0.05	141.2	26.2	1.8	2.0	24	-1.94	0.09	2.08	0.16	-0.15	0.16	-1.09	0.09	-1.80	0.09	0.29	0.15
134	8	7	79	8	55	53.8	5.4	1.1	-22.20	-0.01	0.12	-179.73	-0.15	0.10	600.4	-8.6	7.8	1.5	24	-0.38	0.07	-0.08	0.10	0.45	0.10	-0.13	0.12	-1.02	0.12	-0.32	0.10
135	18	7	79	7	57	48.0	2.7	1.0	-7.67	-0.14	0.10	127.71	0.21	0.11	167.0	-4.0	3.1	2.0	23	9.97	0.97	-7.31	1.11	-2.67	1.20	2.07	0.99	3.99	1.18	4.18	1.23
136*	5	8	79	0	53	55.0	9.1	0.2	-22.95	-0.23	0.03	-177.10	0.39	0.02	229.2	48.2	2.5	4.0	25	-3.49	0.12	1.09	0.14	2.40	0.12	-3.97	0.09	-4.50	0.06	0.32	0.10
137	16	8	79	21	31	31.2	4.9	0.2	41.97	0.16	0.02	131.74	0.95	0.04	604.4	16.4	1.5	3.0	25	6.19	0.19	-1.14	0.23	-5.05	0.27	-0.72	0.30	-9.03	0.29	-4.24	0.24
138	17	8	79	20	19	39.2	3.0	0.5	-4.11	0.26	0.05	128.04	0.17	0.06	259.3	-6.7	3.6	1.5	23	-6.65	0.65	8.08	0.82	-1.43	0.95	1.19	0.76	-9.03	0.73	-6.10	0.97
139	20	8	79	3	51	2.5	10.3	0.5	37.93	1.45	0.08	70.71	0.58	0.05	238.6	9.6	3.8	2.0	24	2.26	0.30	-1.51	0.45	-0.75	0.32	4.48	0.23	0.14	0.32	-0.01	0.40
140	22	8	79	18	28	58.8	3.2	0.4	51.89	-0.38	0.04	158.01	0.68	0.08	126.7	-7.3	2.6	1.5	24	0.69	0.13	0.64	0.21	-1.34	0.20	-1.65	0.13	-3.13	0.14	-2.72	0.20
141	5	9	79	13	56	23.7	5.6	0.4	-27.55	0.00	0.05	-63.08	0.19	0.04	565.6	9.6	2.4	2.0	24	-2.19	0.10	-0.06	0.15	2.26	0.13	-1.22	0.15	1.50	0.16	-0.03	0.13
142	15	9	79	10	2	24.2	11.1	0.8	-15.85	-0.22	0.13	-68.96	0.60	0.09	231.2	17.2	5.6	2.0	24	0.85	0.10	-0.80	0.17	-0.05	0.15	1.42	0.10	-0.73	0.13	0.07	0.14
143	4	10	79	19	41	20.8	2.1	0.8	-7.32	0.10	0.08	128.10	-0.21	0.12	127.7	-16.3	3.5	2.0	23	6.34	0.78	-7.61	0.77	1.27	1.02	0.47	0.58	0.66	0.64	-0.93	0.99
144	5	10	79	16	43	22.4	6.2	0.6	-3.47	0.08	0.06	-75.85	0.42	0.09	132.1	16.1	2.9	2.0	23	-9.78	0.63	0.65	1.09	9.14	1.26	-2.30	0.51	-0.72	0.64	-1.30	0.91
145	11	10	79	12	41	1.9	1.2	0.3	3.80	0.01	0.04	126.13	0.11	0.04	118.7	-6.3	2.8	2.0	24	-0.48	0.08	-0.22	0.13	0.70	0.14	-0.27	0.08	2.30	0.08	-0.21	0.12
146	17	10	79	5	43	14.4	11.7	0.2	18.28	-0.24	0.03	145.37	0.09	0.02	581.2	-19.8	1.6	4.0	26	-1.88	0.05	-0.95	0.08	2.83	0.08	-1.14	0.08	-0.64	0.08	-1.04	0.08
147	20	10	79	23	36	9.9	8.2	1.2	-7.60	-0.23	0.11	128.45	0.29	0.14	165.1	25.1	4.0	2.0	23	8.42	1.33	-8.82	1.21	0.41	1.46	2.95	1.22	6.78	1.46	7.40	1.78
148	30	10	79	1	37	11.2	5.1	0.3	18.68	-0.11	0.04	145.27	0.14	0.02	578.7	-0.3	1.7	4.0	25	-1.41	0.04	-0.48	0.06	1.90	0.06	-0.52	0.07	-1.11	0.08	-0.19	0.07
149*	5	11	79	1	51	15.8	2.9	0.2	17.96	0.13	0.02	-68.46	0.16	0.03	78.3	-25.7	1.9	3.0	25	1.85	0.05	-1.55	0.07	-0.30	0.08	-1.70	0.06	0.23	0.06	0.10	0.06
150	6	11	79	1	25	4.9	4.0	0.3	-21.08	0.00	0.03	-178.98	-0.03	0.04	596.1	7.1	2.3	1.5	24	-2.99	0.09	1.81	0.15	1.17	0.15	-1.52	0.17	-1.92	0.16	0.76	0.14

Table 2. Principal axis representation and 'best double couple' derived from the CMT solutions listed in Table 1. The eigenvalues of the moment tensor are scaled by a factor 10^{EX}. The headings are explained in the text.

NO.	SCALE FACTOR	*** T-AXIS VAL	PL	AZM	N-AXIS VAL	PL	AZM	P-AXIS VAL	PL	AZM	**** MO	BEST DOUBLE COUPLE **N. P. 1** STK	DP	SLIP	**N. P. 2** STK	DP	SLIP
1	10**24	8.38	26	3	-1.32	15	100	-7.06	60	217	7.72	63	23	-130	285	73	-75
2	10**24	1.24	21	28	0.28	46	141	-1.52	36	282	1.38	70	48	-167	332	80	-43
3	10**24	8.83	61	76	-0.21	28	240	-8.62	7	334	8.73	92	46	132	220	58	56
4	10**25	1.27	27	67	0.04	3	158	-1.31	63	255	1.29	149	18	-100	339	72	-87
5	10**24	2.99	50	109	-0.86	31	335	-2.13	23	230	2.56	277	35	27	164	75	122
6	10**26	1.13	42	249	0.13	7	153	-1.26	47	56	1.20	41	7	-23	153	87	-97
7*	10**27	2.13	73	151	-0.27	2	54	-1.86	17	323	1.99	50	28	86	235	62	92
8	10**26	2.51	58	86	0.34	13	198	-2.86	29	295	2.69	58	20	132	194	75	76
9	10**23	7.67	15	280	0.85	51	30	-8.52	35	179	8.10	325	54	-165	226	78	-37
10	10**25	1.11	47	245	0.00	10	346	-1.11	41	85	1.11	237	10	161	346	87	80
11	10**25	1.48	35	132	0.25	51	281	-1.73	16	31	1.60	165	53	164	265	77	38
12	10**24	4.91	54	53	0.53	24	181	-5.45	25	283	5.18	53	29	146	174	74	65
13	10**24	5.39	12	142	-0.52	15	236	-4.87	70	15	5.13	213	35	-117	65	59	-72
14	10**24	0.89	24	150	0.32	25	48	-1.21	54	277	1.05	279	31	-34	40	73	-116
15*	10**25	6.39	25	60	-0.58	15	157	-5.81	60	275	6.10	121	24	-129	342	72	-74
16	10**24	2.91	19	93	0.11	2	184	-3.02	71	278	2.96	180	26	-94	4	64	-88
17*	10**25	1.80	20	193	0.22	46	81	-2.03	37	299	1.91	329	48	-15	70	79	-137
18*	10**25	4.03	47	161	-0.39	42	329	-3.64	6	64	3.84	191	54	147	302	64	41
19	10**24	4.14	87	65	-0.92	0	158	-3.22	3	248	3.68	338	42	90	158	48	90
20	10**25	1.49	54	52	0.08	7	307	-1.57	25	214	1.53	289	21	71	130	70	97
21	10**25	2.25	18	61	0.20	43	169	-2.45	42	314	2.35	107	46	-160	3	75	-46
22	10**24	1.35	21	189	-0.45	63	331	-0.90	15	93	1.13	230	64	175	322	86	26
23	10**24	5.22	37	94	2.40	23	203	-7.62	44	317	6.42	123	23	-170	24	86	-67
24	10**24	9.27	10	271	-0.85	10	180	-8.42	76	45	8.85	14	36	-73	173	56	-102
25-	10**28	1.43	34	286	-0.08	1	17	-1.35	56	107	1.39	14	11	-93	197	79	-89
26	10**24	0.81	10	117	0.42	31	213	-1.23	57	10	1.02	175	44	-137	51	62	-55
27	10**25	2.37	17	94	-0.05	33	196	-2.32	52	341	2.34	146	40	-148	30	70	-55
28	10**24	2.44	9	211	-0.18	11	119	-2.27	75	340	2.36	315	37	-71	112	55	-104
29	10**25	1.57	51	135	-0.34	39	313	-1.23	1	44	1.40	166	56	140	282	58	42
30	10**24	4.40	31	307	-0.34	11	44	-4.05	57	152	4.23	5	18	-130	227	77	-78
31	10**25	1.17	53	149	-0.28	36	309	-0.88	10	46	1.02	171	47	143	288	64	50
32	10**24	3.52	56	187	0.88	22	59	-4.40	24	319	3.96	11	29	38	247	73	114
33	10**25	3.84	33	129	0.19	12	227	-4.02	54	334	3.93	181	16	-137	49	79	-78
34	10**24	1.56	56	291	-0.30	20	169	-1.26	26	69	1.41	121	26	39	355	74	110
35	10**24	3.89	21	108	2.07	1	18	-5.96	69	235	4.92	201	24	-87	17	66	-91
36	10**24	1.78	17	104	-0.19	10	197	-1.59	70	317	1.69	179	29	-111	22	63	-79
37	10**24	5.58	65	157	-0.90	24	349	-4.79	5	257	5.19	323	45	55	188	54	120
38	10**24	2.63	10	275	-0.39	17	9	-2.24	70	157	2.43	345	38	-119	200	57	-69
39*	10**26	2.07	47	242	-0.84	3	335	-1.24	43	68	1.65	206	4	141	335	88	87
40	10**25	1.60	8	205	-0.13	57	307	-1.47	32	110	1.53	252	62	-162	154	74	-29
41	10**24	5.85	26	197	1.50	33	88	-7.34	46	316	6.60	334	35	-20	81	79	-124
42	10**25	2.34	25	152	-0.40	64	317	-1.94	6	59	2.14	192	68	166	288	77	22
43	10**24	1.61	66	123	-0.55	24	286	-1.06	6	19	1.34	133	44	125	269	55	61
44	10**24	4.28	42	59	-0.46	44	211	-3.83	14	315	4.05	88	49	157	193	72	43
45	10**24	2.95	68	108	-0.03	21	307	-2.92	6	214	2.93	283	43	59	142	55	115
46	10**24	7.29	39	120	0.20	5	26	-7.49	50	289	7.39	249	8	-47	25	84	-95
47	10**24	6.40	39	159	0.76	12	59	-7.16	49	315	6.78	304	13	-24	58	85	-102
48	10**24	4.95	30	167	1.27	12	69	-6.22	57	320	5.58	290	18	-48	66	76	-103
49	10**24	1.10	77	307	-0.28	9	79	-0.82	9	171	0.96	271	36	105	73	55	79
50	10**24	2.56	22	100	0.22	28	202	-2.78	53	337	2.67	150	34	-148	32	73	-60
101	10**25	1.13	11	359	0.19	2	90	-1.32	79	189	1.22	87	34	-93	271	56	-88
102	10**24	7.39	48	108	0.22	11	211	-7.61	40	311	7.50	100	12	160	210	86	79
103	10**24	7.63	45	58	0.16	39	204	-7.78	18	309	7.70	82	44	156	190	74	49
104	10**24	8.46	39	62	-0.77	25	310	-7.68	40	196	8.07	218	25	-2	309	89	-115
105	10**24	0.98	6	223	0.04	39	128	-1.02	50	320	1.00	348	52	-37	102	62	-136
106	10**24	4.05	46	277	-0.27	44	105	-3.78	4	11	3.92	65	56	33	315	63	141
107	10**24	1.75	36	86	-0.01	2	354	-1.74	54	261	1.74	187	9	-77	354	81	-92
108	10**24	7.01	38	49	0.21	45	189	-7.21	21	301	7.11	79	47	166	179	80	44
109	10**25	4.75	76	100	-0.51	3	203	-4.24	14	294	4.49	29	31	96	201	59	86
110	10**24	1.94	59	210	-0.26	7	312	-1.68	30	47	1.81	158	17	117	310	75	82
111	10**25	2.85	60	210	-0.28	29	17	-2.56	6	110	2.71	229	47	132	356	57	54
112	10**25	1.35	73	77	0.30	4	180	-1.64	17	271	1.50	7	29	98	178	62	86
113	10**24	2.34	17	243	0.00	71	86	-2.35	7	335	2.34	20	73	8	288	83	163
114	10**24	1.24	2	191	-0.47	38	99	-0.76	52	283	1.00	313	54	-41	70	58	-136
115	10**24	7.75	31	253	0.36	14	352	-8.11	56	104	7.93	306	19	-138	175	77	-75
116	10**24	1.02	46	168	-0.19	44	342	-0.84	3	75	0.93	201	57	146	311	62	38
117	10**25	7.81	24	50	0.90	25	152	-8.72	54	282	8.27	100	31	-146	340	74	-64
118	10**23	5.96	7	308	1.92	80	175	-7.88	7	39	6.92	84	80	0	174	90	-170
119	10**25	2.49	23	158	0.58	4	249	-3.06	66	350	2.78	238	22	-102	71	69	-85
120	10**23	9.61	49	350	-0.06	3	84	-9.55	40	177	9.58	299	6	125	84	85	87
121	10**24	8.38	28	31	-0.42	56	176	-7.96	16	292	8.17	69	58	171	164	82	33
122	10**25	1.30	48	152	-0.12	42	325	-1.18	4	58	1.24	183	55	145	295	62	40
123	10**25	1.24	42	84	-0.21	17	338	-1.03	43	231	1.14	246	17	-2	338	89	-107
124	10**24	1.85	58	19	1.32	25	157	-3.17	19	256	2.51	20	34	139	146	68	63
125	10**25	5.34	2	149	0.32	2	58	-5.66	87	285	5.50	240	43	-87	57	47	-93
126	10**26	2.46	44	354	0.02	15	99	-2.49	43	203	2.47	6	15	178	99	89	75
127	10**25	1.08	29	193	0.30	16	292	-1.38	56	46	1.23	245	21	-138	115	76	-74
128	10**24	3.52	40	189	-0.74	0	279	-2.78	50	10	3.15	276	5	-94	99	85	-90
129	10**24	4.58	25	161	0.06	13	257	-4.63	61	12	4.60	224	23	-125	81	71	-76
130*	10**26	2.89	9	67	0.06	34	331	-2.95	55	169	2.92	190	47	-40	310	62	-129
131*	10**26	0.94	13	30	0.14	8	298	-1.08	75	179	1.01	131	32	-76	294	59	-99
132	10**24	1.41	12	187	-0.14	1	278	-1.27	78	14	1.34	276	33	-92	99	57	-88
133	10**24	2.60	20	161	0.57	23	62	-3.17	59	287	2.88	284	32	-43	52	69	-115
134	10**24	1.17	32	79	-0.03	18	181	-1.14	52	295	1.15	123	21	-149	4	80	-72
135	10**24	1.17	69	299	-0.19	21	120	-0.98	1	30	1.07	101	48	62	320	49	118
136*	10**25	6.01	32	124	1.31	5	217	-7.31	57	315	6.66	195	14	-112	38	77	-85
137	10**26	1.14	59	76	0.03	16	196	-1.16	26	294	1.15	56	24	133	190	73	73
138	10**24	1.27	17	34	0.12	34	136	-1.38	50	282	1.32	84	41	-150	330	71	-53
139	10**24	5.24	56	358	-0.75	0	88	-4.49	34	178	4.86	269	11	91	88	79	90
140	10**24	3.05	44	67	2.26	31	192	-5.31	30	303	4.18	86	32	166	188	82	59
141	10**24	2.77	19	261	0.33	17	165	-3.10	64	35	2.94	17	31	-54	157	66	-109
142	10**24	1.86	57	35	-0.13	8	293	-1.74	31	198	1.80	263	15	60	114	77	98
143	10**23	6.43	83	282	1.30	7	94	-7.73	2	174	7.08	271	43	100	78	48	81
144	10**24	0.93	1	82	0.10	12	172	-1.03	77	347	0.98	159	45	-108	4	47	-73
145	10**24	2.52	38	261	-0.26	2	353	-2.26	52	86	2.39	336	8	-107	173	83	-88
146	10**26	3.12	4	77	-0.25	37	170	-2.87	52	341	2.99	134	52	-140	17	59	-45
147	10**24	1.41	52	297	-0.11	38	122	-1.30	2	30	1.35	88	54	41	331	58	136
148	10**25	2.23	17	89	-0.28	20	186	-1.95	64	322	2.09	152	33	-128	15	65	-68
149*	10**25	2.57	67	189	-0.29	1	96	-2.28	23	6	2.42	93	22	87	277	68	91
150	10**24	3.22	21	140	0.75	6	48	-3.97	68	303	3.60	241	24	-76	45	66	-96

The individual elements of the moment tensor and their standard errors, listed in Table 1, are scaled by a factor 10^{EX} dyne cm; the exponent EX can be found in the corresponding column.

For a few events the epicentral position or the depth have been held fixed in the inversion. Generally, these are cases for which the centroid epicentral coordinates were too

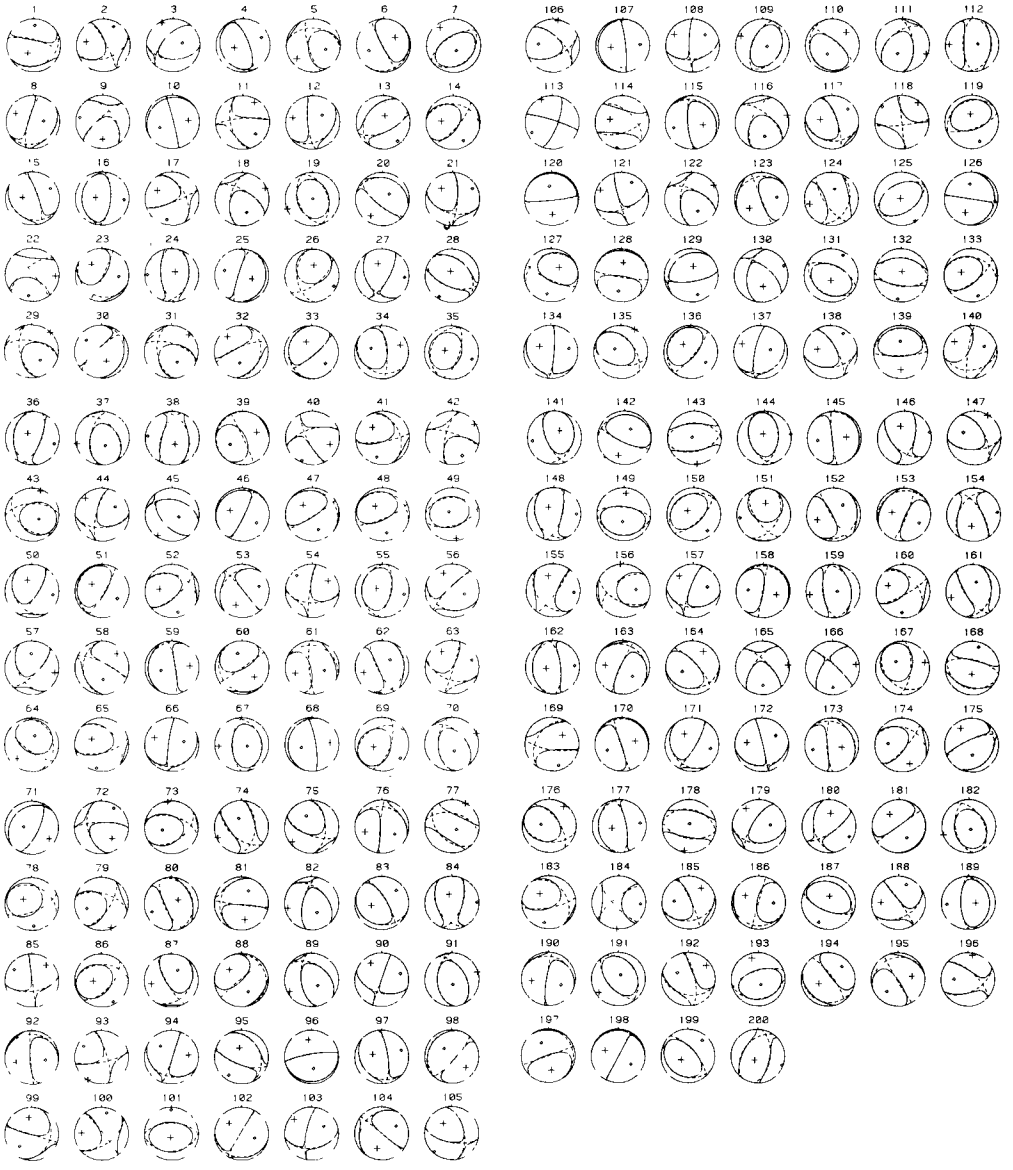

Figure 5. Focal mechanisms of the 200 CMT solutions. The 'complete' moment tensor (continuous lines) and the 'best double couple' (dashed lines) are shown for each solution. For both representations the lines separate the expected compressional first arrivals of *P*-waves from the expected dilatational arrivals. The compression axis is indicated with '+'. Events with a large deviation from the double couple model can be identified by the poor fit between the complete moment tensor and the best double couple. The difference can be extreme for events having a mechanism close to a vector dipole (e.g. solutions 26 and 43). The numbering of events is the same as that in Tables 1 and 2.

far from the original location or for which the solution was unstable. Most of these events are characterized by a very poor azimuthal coverage of stations. A typical example is the 1977 June 3 event in the Hindu Kush region, for which only four stations could be used.

Table 2 lists some parameters derived from the moment tensors: the eigenvalues, the principal axes, and the orientation of the nodal planes for the 'best double couple'. The tension axis (T) is associated with the largest positive eigenvalue, the compression axis (P) with the maximum negative and the null axis (N) with the intermediate eigenvalue. The best double couple (M_0, 0, $-M_0$) is constructed by taking M_0 as the average (in absolute values) of the dominant eigenvalues, and taking the eigenvector corresponding to the intermediate eigenvalue to be the direction of the null axis.

Fig. 5 shows the equal area projection of the lower focal hemisphere, corresponding to the complete moment tensor (solid lines), and, superimposed, the best double couple for each solution (dashed lines). We prefer this representation because it indicates how the procedure of fitting the moment tensor with a double couple is, sometimes, quite inadequate (e.g. events 26 and 43). For such events the question arises as to whether the double couple is really an appropriate way of representing the seismic source and if, by imposing the double couple mechanism, we are masking some important properties of the failure process.

In Table 2, the convention of Aki & Richards (1980) has been used in defining the strike, dip and slip angles for the nodal planes of the best double couple.

Statistical properties of the CMT solutions

(a) EPICENTRAL COORDINATES

The waveform data used in the CMT method are affected by the lateral heterogeneity of the Earth, especially for earthquakes located at the boundaries between plates. Therefore the CMT epicentre cannot be interpreted as a 'relocated' epicentre. If the lateral heterogeneity is the factor that most affects the centroid position, we would expect to see consistency in the epicentral shifts; earthquakes in the same region should shift in the same direction. Indeed, this consistency is verified by our solutions. Fig. 6(a) shows the epicentre relocation vectors for all the intermediate depth events with moment larger than 10^{25}. Each arrow points from the NEIS position to the CMT epicentre and has been magnified by a factor of 30. There is an obvious consistency in most subduction zones both in the direction and amplitude of the shifts. The situation is more confused in New Guinea and Philippine Islands regions, characterized by a very complex tectonic setting and where the amplitude of the relocation vectors is smaller.

Fig. 6(b) shows epicentre shifts for deep events with moments larger than 10^{25}; the amplitude of the shift is generally smaller for deep events, and shows less consistency in direction. This indicates that the effect of lateral heterogeneity is less important for deep events. The epicentre positions are also affected by mislocation of the NEIS epicentres and by discrepancies introduced by assuming a point source instead of a source distributed in space and time.

(b) DEPTH

In the CMT method the depth phases, p and s, do not have to be individually identified, but are automatically included in the traces used for the inversion. Thus, the CMT estimate of the depth is, on average, more reliable than the depth reported by the NEIS.

Fig. 7 shows a plot of NEIS depths versus CMT depths. The deviation can be quite large, and there is an average shift for deep events: CMT locations tend to be deeper than NEIS

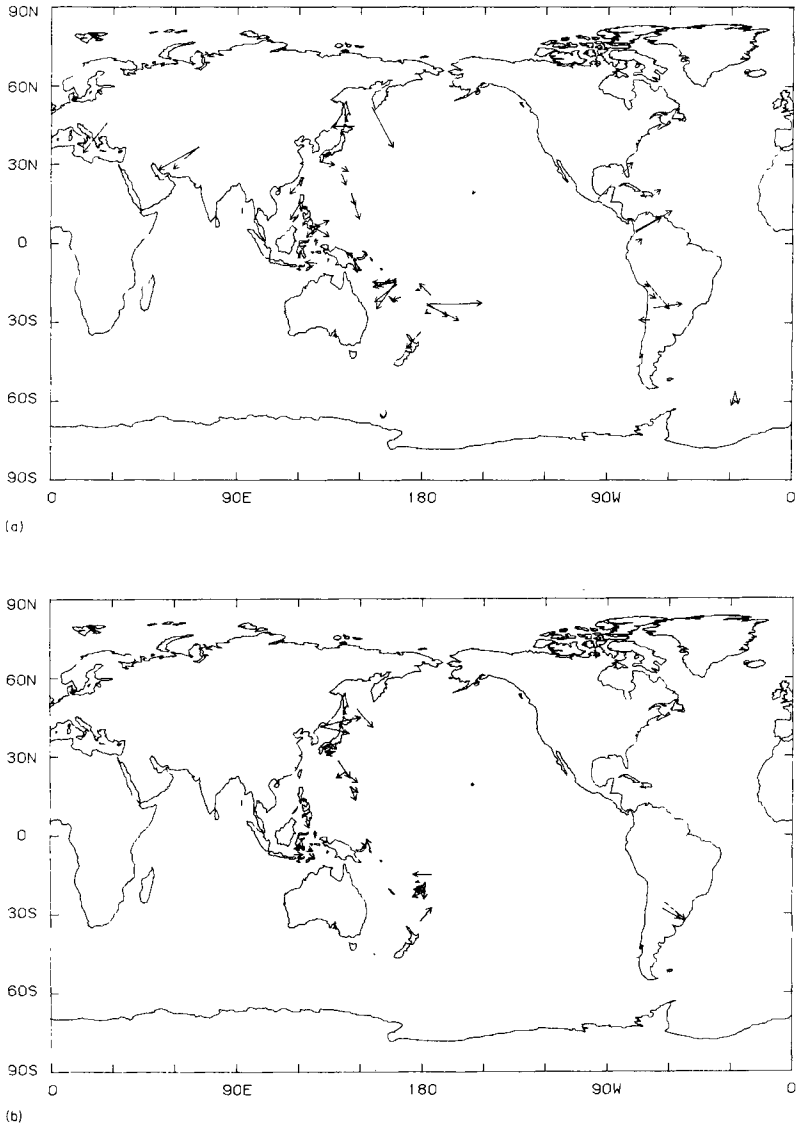

Figure 6. (a) Shift of the centroid epicentral locations with respect to the NEIS epicentres for events shallower than 300 km and moment larger than 10^{25} dyne cm. The length of the arrow is proportional to the magnitude of the shift magnified by a factor of 30. (b) Same as (a) but for events deeper than 300 km.

hypocentres. Dziewonski & Woodhouse (1983) pointed out that this effect depends on the difference between the PREM model, used for CMT, and the Jeffreys–Bullen travel times used in the NEIS hypocentre determination; the PREM model is faster at depths between 400 and 700 km.

Particularly interesting is the group of events with NEIS depth shallower than 100 km, which show large depth shifts in the CMT locations. These are events with moments larger than 10^{27}, which have a large vertical extent, as it will be shown in a later section. For these events the centroid position differs from the NEIS position because of source finiteness.

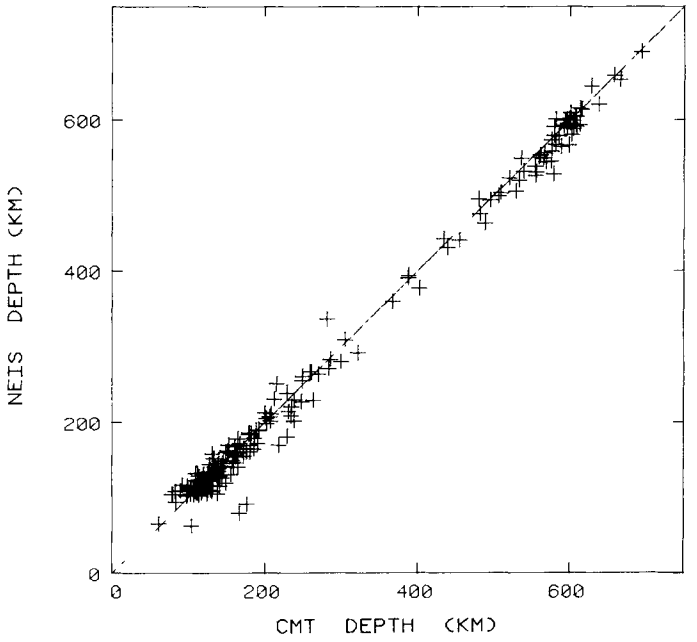

Figure 7. Comparison of NEIS depth versus CMT depth for the 300 analysed events.

(c) ORIGIN TIME

The centroid time represents the time shift between the centroid and the source time given by the catalogue. It is primarily connected to the source duration and to the changes in epicentral coordinates and centroid depth; if the latter are large, the time shift will not be a good estimate of the source half-duration.

Fig. 8(a) shows the origin time shifts as a function of the logarithm of the seismic moment for events shallower than 300 km. Both the high scatter of the distribution and the increase of the shift with moment are clear. The distribution has been fitted with a curve $\delta t_0 = A + B \times M_0^{1/3}$, with the assumption of proportionality between fault length and the cube root of seismic moment (Kanamori & Anderson 1975). The scatter is to be attributed partly to the shifts in the hypocentral coordinates of the centroid solutions and partly to source complexities that cannot be resolved by an analysis of the first-order source parameters. A similar result was obtained by Furumoto & Nakanishi (1983) in a source time analysis of 14 large shallow events; their value for the constant B (1.7×10^{-8}, derived from $M_0 = 2.5 \times 10^{22} \tau^3$, where τ is the source time), is identical to that obtained in this study making use of intermediate size earthquakes.

The distribution for deep events, Fig. 8(b), is markedly different. The average origin time shift is almost constant throughout the range of moments. By fitting the distribution with the same curve we obtain a very high value for the constant A, 5.9 s; this can be only partially explained by the average depth shift of the CMT hypocentres, and is interpreted as an indication of the complexity and the multiple shocks nature of the rupture process in deep events. The smaller scatter of this distribution can be due to the fact that shifts in hypocentral parameters are smaller for deep events, as we noted above. In Fig. 8(b) we also plot the source time values for four large deep events analysed by Furumoto & Nakanishi (1983); these values are only slightly higher than predicted by our distribution and confirm

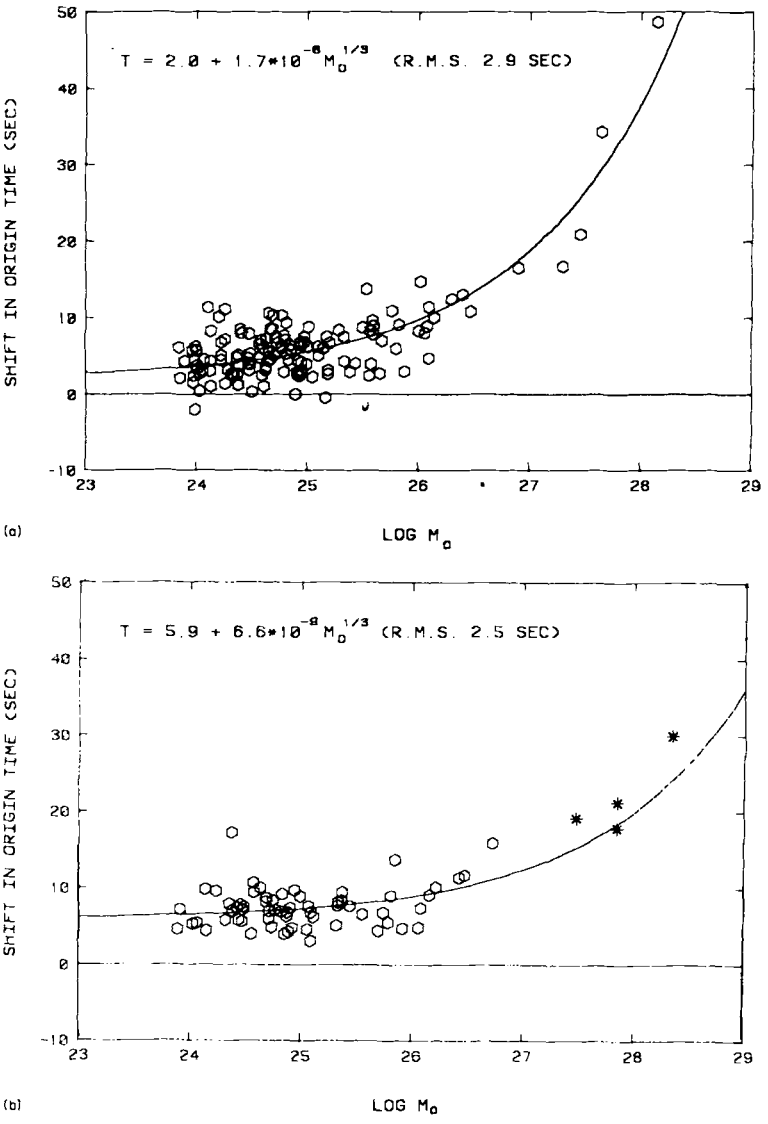

Figure 8. (a) Shift in the origin time versus $\log_{10} M_0$ for events shallower than 300 km. The least squares line with exponent 1/3 is shown. (b) Same as (a) but for deep events ($h > 300$ km). The stars are for the events nos 4, 21, 25 and 30 in the list of Furumoto & Nakanishi (1983). Only the CMT solutions have been used to obtain the best fitting curve.

the small dependence of the source duration on the seismic moment for deep events. An analogous analysis performed by Dziewonski & Woodhouse (1983) gave very similar results to ours, apart from a smaller constant A for shallow and intermediate depth events.

We would like to comment on the difference between the two time parameters used by the CMT method: source duration and shift in origin time (both listed in Table 1). The source duration T is an input parameter for the CMT and is not modified during the inversion. It is used in multiplying the synthetic spectra by $(\sin \omega T)/\omega T$, where ω is frequency. This is done with the purpose of estimating the moment tensor at 0 frequency, thus independently of the data used. The source duration parameter represents the assumed

half-duration of the source as inferred from the moment on the basis of a law of the form $\delta t_0 \sim M_0^{1/3}$ with the implicit assumption of a simple seismic source. The shift in origin time, on the other hand, locates the centroid respect to the initial time of the event given by the catalogue.

In the first inversion of the CMT, origin time and source duration are roughly estimated from the magnitude of the event and the observed amplitude of the signal, and used as input parameters. The shift in origin time and the source duration (derived from the moment) obtained in the first iteration are then used in the second iteration.

Neither the source duration nor the shift in origin time can be considered estimates of the real half-duration of the source. The former is derived from an empirical relation without knowing anything about the time history of the source. The latter is biased by shifts in hypocentral coordinates, sometimes quite large, and by possible catalogue mislocation; moreover, it locates the centroid and not the half-point of the source time function, which can be very different in the case of complex events.

It is interesting to notice that for small and intermediate events, the scalar moment is not too sensitive to the source duration used, because $(\sin \omega T)/\omega T$ tends to 1 for small T. The problem becomes primary for large events ($T > 10$ s), generally characterized by complex time history and for which the empirical relation found in Fig. 8 is very uncertain. A change in source duration between 20 and 30 s, for example, results in a large increase in the seismic moment. For these events the source duration is chosen so that the 0 frequency moments obtained separately from body and mantle waves are equal.

(d) MAGNITUDE SCALE m_b

The problem of the quantification of deep earthquakes has been long debated and yet not successfully resolved (see, e.g. the Proceedings of the Workshop on Quantification of Earthquakes held as part of the General Assembly of IASPEI, London, Ontario, 1981 July).

The first magnitude scale introduced for deep earthquakes is the body-wave magnitude m_B (Gutenberg 1945), which makes use of various seismic phases such as *P*, *PP* and *S*.

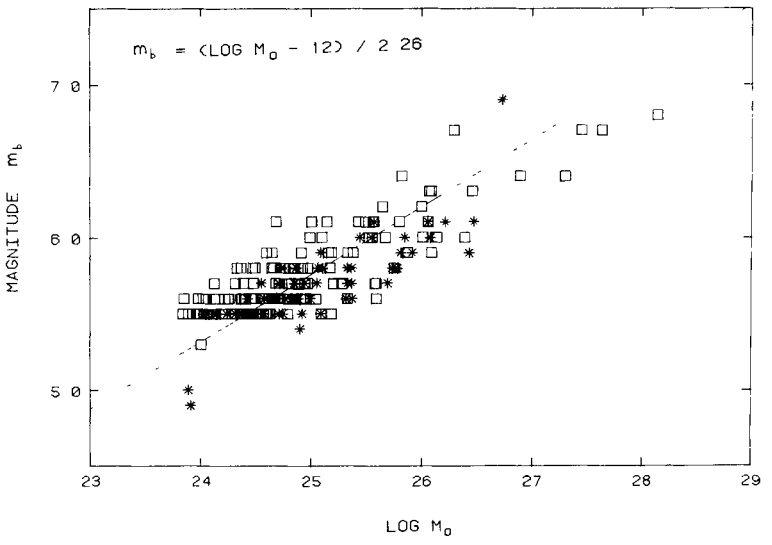

Figure 9. Body-wave magnitude m_b displayed as function of $\log_{10} M_0$. Events shallower than 300 km are indicated with squares; deeper events with stars. See explanations in the text for the best fitting line.

Recently, m_B has been estimated for major intermediate depth and deep events using waves with periods between 4 and 15 s (Abe & Kanamori 1979; Abe 1982). An empirical relation between m_B and seismic moment was found (Abe 1982; $m_B = (\log M_0 - 10)/2.4$) to coincide with a theoretical moment magnitude, m_w, proposed by Kanamori (1983) by combining the magnitude–energy relation $\log E = 2.4 \times m_B + 5.8$ (Gutenberg & Richter 1956) and the energy–moment relation $E = M_0/(2 \times 10^4)$ (Vassiliou & Kanamori 1982). Until now, however, m_B has been determined only for very large events, and, since the installation of the World-Wide Standardized Seismograph Network (WWSSN), the more common scale in use has been the body-wave magnitude m_b, routinely determined from short-period *P*-wave arrivals at a period of 1 s. It was recognized that this scale has a saturation limit, owing to its high-frequency character, and cannot adequately measure the size of large events. Also, because of the use of *P*-waves alone, m_b is more strongly related to the source mechanism, although this is more the case for shallow events than for deep events, whose mechanisms seldom are of the strike-slip type.

The seismic moment M_0 is the parameter that best estimates the size of earthquakes. It is routinely retrieved for all the events with $M_0 > 10^{24}$, some 300 events each year (e.g. Dziewonski & Woodhouse 1983). However, this systematic operation cannot be done for events before 1977, owing to the lack of an adequate source of digitized waveform data. Therefore, the magnitude m_b remains the more common magnitude scale in use and a relation between m_b and M_0 is of primary importance in studies of seismicity based on the magnitude scale. Our dataset provides us with an excellent possibility to test such relation.

A plot of m_b versus $\log_{10} M_0$ is shown in Fig. 9. The scatter of the distribution is large. For a given value m_b the corresponding moments vary by two orders of magnitude for intermediate depth events (indicated with □); deep events (*) show, on average, smaller magnitude values and less scatter, slightly more than one order of magnitude.

It is clear in Fig. 9 that by taking as our minimum threshold value $m_b = 5.5$ we have omitted a large number of events with moments between 7×10^{23} and 10^{25}. A few exceptions can be identified in Fig. 9 with m_b around 5.

Due to the fact that our dataset is not complete for lower moments, the simple interpolation of the data by a line would not be correct, since such a line would be biased towards higher magnitudes for small values of moment. Instead, we notice that our data sample is bounded on the upper and lower sides by two parallel lines with slope approximately equal to 0.44. Lacking a more complete set of results, we choose an intermediate line between the two boundaries to represent m_b as function of the seismic moment

$$m_b = (\log M_0 - 12)/2.26.$$

This relation agrees with the empirical relation reported by Kanamori (1983, fig. 4b; derived from Noguchi & Abe 1977), for $m_b < 6$. However, we do not find any evidence of saturation of the m_b scale for $m_b > 6$, although our sample is incomplete for $M_0 > 5 \times 10^{26}$. Also, the scatter of the distribution for deep events is only slightly larger than the scatter of the distribution of m_B versus M_0 reported by Abe (1982, fig. 1) for events with $M_0 > 10^{25}$. These results indicate that the magnitude scale m_b, even though affected by larger scatter, provides an estimate of the size of deep earthquakes not dissimilar from that obtained using the broad-band body-wave magnitude scale m_B.

(e) DEVIATION FROM THE DOUBLE COUPLE MODEL

We recall that the CMT solution is retrieved with the condition $\mathrm{Tr}(M) = 0$, but not constraining the mechanism to be a double couple. Thus, only two of the eigenvalues

(M_1, M_2, M_3) of the symmetric moment tensor M are independent; $M_3 = -M_1 - M_2$. If the earthquake mechanism is a plane shear, or double couple, $M_2 = 0$. In general this is not the case, and we can measure how much the mechanism deviates from the double couple by taking

$$\epsilon = M_2/\mathrm{MAX}(|M_1|, |M_3|).$$

The absolute value of ϵ may range between 0, corresponding to a double couple, and 0.5, in which case $M_2 = \mathrm{MIN}(|M_1|, |M_3|)$, corresponding to equal major and minor double couples in the terminology of Gilbert (1981) or to the linear vector dipole proposed by Knopoff & Randall (1970). Some good visual examples of moment tensors with $\epsilon = 0$ or ϵ close to 0.5 can be seen in Fig. 5; as we noted before, the difference between these two cases is striking.

Attempts have been made to analyse the behaviour of ϵ as a function of seismic moment, depth and regional distribution (e.g. Dziewonski & Woodhouse 1983; Giardini 1983). We limit ourselves in this study to showing some general properties of the deviation of our

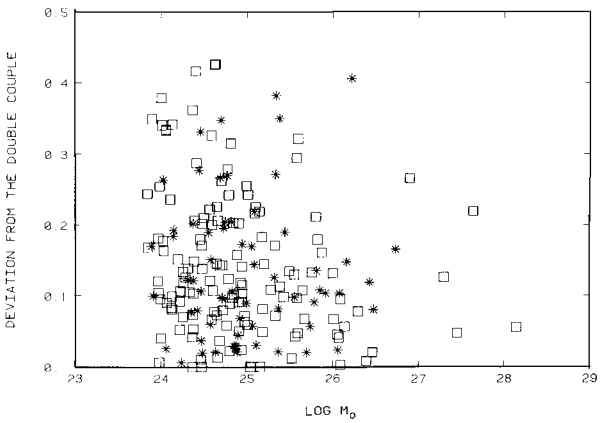

Figure 10. Deviation from the double couple model as a function of seismic moment. Events shallower than 300 km are indicated with squares, deeper events with stars.

solutions from the double couple. Fig. 10 shows a plot of ϵ versus the logarithm of the seismic moment. The scatter of the distribution is very high, but, on average, ϵ decreases with increasing moment. We do not find any evidence of a different behaviour of intermediate depth solutions (indicated in Fig. 10 with □) compared to deep events (∗).

Fig. 11 plots ϵ versus CMT depth. The deviation is taken as positive if the dominant eigenvalue, the larger in absolute value, is associated to the compression axis, negative if to the tension axis; larger symbols correspond to larger moments. Again, the scatter of the distribution is quite large, especially for depths around 150 and 600 km. Nonetheless, interesting indications can be drawn from the sign of ϵ. Two-thirds of the events deeper than 350 km have positive deviation, corresponding to a predominance of the compression axis. This could be related to the fact that deep subducting slabs are dominated by down-dip compression (in the terminology of Isacks & Molnar 1971).

A regional analysis shows a much stronger correlation between the sign of ϵ and the state of stress of the subducting slabs. Fig. 12(a) shows the deviation for the CMT solutions in Sandwich Islands subduction zone. This region is characterized by shallow seismicity and by events with the T-axis in the direction of the slab dip. Our results not only confirm that

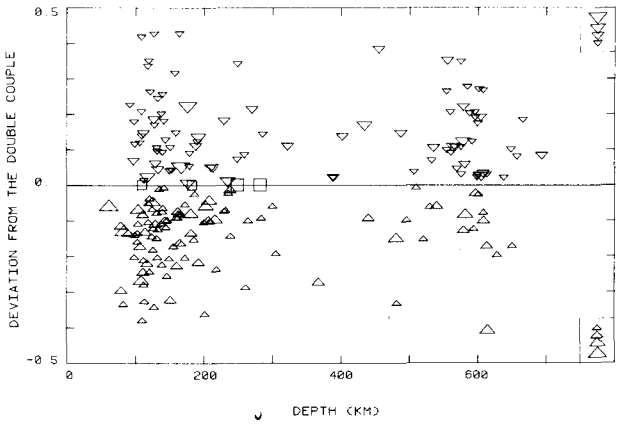

Figure 11. Deviation from the double couple displayed as a function of depth. The deviation is taken as positive if the larger eigenvalue, in absolute values, is associated with the compression axis, negative if with the tension axis. Squares indicate events with a perfect double couple mechanism. The size of the symbols (plotted in the right corners of the figure) is proportional to the seismic moment; threshold values are 10^{25}, 10^{26} and 10^{27} dyne cm.

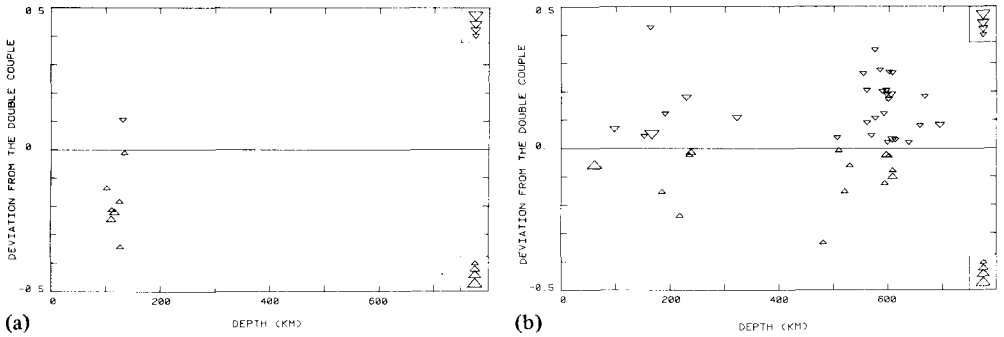

Figure 12. (a) Same as Fig. 11 but for earthquakes in the Sandwich Islands subduction zone. The same events are shown in Fig. 14(b). (b) Same as Fig. 11 but for earthquakes in the Tonga Islands subduction zone. The same events are shown in Fig. 14(a).

this region is in down-dip tension, but show that the eigenvalue associated with the *T*-axis is also dominating most of the moment tensor solutions. An opposite case is shown in Fig. 12(b); all the events from the Tonga subduction zone are included. This region is known for the strong deep seismicity and the general alignment of the *P*-axis with the dip direction (e.g. Isacks & Molnar 1971). Again, not only is this slab in down-dip compression, but three-quarters of the moment tensor solutions are dominated by the compressional eigenvalue.

The interpretation of the deviation from the double couple model is still very tentative and controversial (e.g. Dziewonski & Woodhouse 1983). The high scatter of the results is the main obstacle to a clear understanding. However, some undeniable cases of consistent behaviour of ϵ have been shown; for example, compare the high state of tension recognized by Ekström & Dziewonski (1983) in the Mammoth Lakes earthquakes sequence. Also, strong evidence has emerged that some shallow events, characterized by a large deviation from the double couple and by disagreement between the CMT solution and first-motion fault plane mechanism, consist of separate rupture episodes on different faults (Jackson

1983, private communication). These studies, as well as our results, lead us to believe that the deviation from the double couple contains important indications about properties of the seismic source and merits further investigation.

Events of particular interest

The object of this study is a systematic analysis of seismicity; however, some events are worthy of particular investigation. These include events with moments larger than 10^{27} as well as two very small events. For some of these the moment tensor has also been determined by other authors using different techniques. In comparing the CMT solutions with moment spectra (e.g. Silver & Jordan 1983), we will retain the seismic moments as 0 frequency moments, as explained above, with the assumption of the correct choice of the source duration. Also, lacking a more valid estimate of the duration of the source rupture, we will consider the shift in origin time as a measure of half the duration of the source.

(a) TONGA ISLANDS, 1977 JUNE 22

This normal fault earthquake was located toward the southern part of the Tonga Arc. It is the largest intermediate depth event in the period 1977–80, and the largest for which a CMT solution has been obtained. Although the NEIS catalogue reports a depth of 65 km, we included this event in our study because of indications in the literature of uncertain depth. The distribution of the aftershocks can be fitted with a plane striking 192° and dipping 63°, and extends down to a depth of 166 km (Silver & Jordan 1983). On the other hand, Talandier & Okal (1979), using *pP-P* readings, suggested a depth shallower than 50 km. Also, reports (NEIS) of tsunami generation, with amplitudes of 40 cm at Suva and 12 cm at Papeete, indicate that the fault reached the surface. The CMT solution obtained only with body waves converges to 130 km depth; however, these body waves are strongly affected by non-linearity, as discussed above. The CMT solutions obtained using mantle waves from GDSN and IDA give similar depths of about 60 km. An attempt to merge the body and mantle waves dataset resulted in a substantial decrease in moment at an intermediate depth. Thus, we chose the mantle wave solution; this was the only case, in our sample, for which body waves were discarded.

Our scalar moment, 1.4×10^{28}, agrees with the result of Talandier & Okal (1979), 1.5×10^{28}, based on Rayleigh waves of period 200 s, and is smaller than the 0 frequency moment, 2.3×10^{28} of Silver & Jordan (1983). The geometry of the best double couple derived from the CMT solution (no. 25 in Fig. 5) indicates a steeper normal fault (79°) than the solutions reported by Silver & Jordan (1983). The shift in origin time, 48 s, is very large (see Fig. 8a), suggesting an episodic rupture process.

(b) ROMANIA, 1977 MARCH 3

This intermediate depth event is by far the largest that has occurred in Europe since 1977. It was a steep thrust event found to consist of three shocks over a 15 s interval and with a fault length of about 60 km (Mueller *et al.* 1978). Our moment, 2×10^{27}, is slightly higher than the moment reported by Silver & Jordan (1983), 1.4×10^{27}, and compares with the one obtained by Hartzell (1979), $1-2 \times 10^{27}$, using surface waves at 18 mHz. The CMT depth, 84 km, is shallower than the depth reported by the NEIS, 94 km. The nodal plane orientations (no. 7 in Fig. 5) confirms the first-motion solution obtained by Mueller *et al.* (1978).

(c) KURILE ISLANDS, 1978 DECEMBER 6

This large intermediate depth event was located on the north of the Hokkaido corner, at the complex junction between the Benioff zones of the southern Kuriles (dipping 45° to the NW) and northern Honshu (dipping 30° to the West). The distribution of the aftershocks forms a distinctive mark in the seismicity between 50 and 200 km of depth. This event has been interpreted as a typical example of slab-tearing, produced by the displacement of the two slabs (Malgrange & Okal 1983; Silver & Jordan 1983). This is a possible mechanism for events in this region (Sasatani 1976), especially at these depths.

It was a complex earthquake, found to consist of three separate episodes on a time span of 70 s (Malgrange & Okal 1983). This could explain the differences existing among the solutions obtained by various authors. Our scalar moment, 4×10^{27}, is in good agreement with the value obtained at 0 frequency by Silver & Jordan (1983), 3.6×10^{27}, but it is lower than the long-period surface wave solution of Romanowicz (1983, private communication), and much higher than the surface waves estimates of Malgrange & Okal (1983) and of Masters & Gilbert (1982, unpublished; reported by Silver & Jordan 1983).

The geometry of the CMT fault plane solution (no. 100 in Fig. 5) agrees with the best fitting plane of the aftershock distribution (obtained by Silver & Jordan 1983); the vertical plane perpendicular to the trench is therefore identified as the fault plane. However, noteworthy differences exist in the orientation of the CMT auxiliary plane with respect to the solutions obtained by Masters & Gilbert and by Romanowicz.

The shift in origin time (34 s) is larger than the predicted (Fig. 8a), and confirms the complex character of the source process.

It is interesting to notice that the CMT solution converges to a depth of 176 km, in the middle of the distribution of the aftershocks and much deeper than reported by the NEIS (91 km) and by the ISC (118 km). The same depth has been obtained by Romanowicz (1983, private communication) using 300 s period surface waves. This large shift in depth can be partially responsible for the variability in the solutions reported above.

We find a similar case of anomalous depth shift for the large shock of 1980 April 13, located in the Tonga Islands region (with $M_0 = 2.8 \times 10^{27}$). Although the Neis lists this event at a depth of 79 km, the CMT solution converges at 166 km. The similarity with the Kuriles event led to identify the approximately vertical focal plane as the fault plane (cf. no. 171 in Fig. 5).

(d) HONSHU, 1978 MARCH 7

This is the largest deep event in our dataset. Geographically associated with the Island of Honshu, it was located in the deeper and more active part of the Benioff zone which dips west of the Bonin Islands. This event has been analysed in several moment tensor studies and offers an excellent opportunity to compare different techniques. The CMT moment, 5.4×10^{26}, confirms the values obtained by Silver & Jordan (1983), 5.2×10^{26}, and by Masters & Gilbert (1979), 5.2×10^{26} (reported also by Gilbert 1981); both authors used long-period IDA data. The duration of the event estimated from the shift in origin time, 32 s, is the same found by Silver & Jordan (1983). A CMT solution was obtained also by Dziewonski *et al.* (1981), using only body waves; their moment is 4×10^{26}. This low value was explained by the authors as due to the finite duration of the source. The use of mantle waves with much longer periods than body waves corrects this effect and allows us to retrieve a solution virtually identical to those obtained with longer-period surface-wave data. Unpublished moment tensor solutions (Masters & Gilbert 1982, reported by Silver & Jordan 1983; Kanamori, reported by Dziewonski *et al.* 1981) are similar to solutions

discussed above. Our fault plane mechanism (no. 62 in Fig. 5) shows a very shallow dipping compression axis, typical of this region, and confirm the mechanisms obtained for this earthquake in other studies.

(e) FIJI PLATEAU, 1977 MARCH 17, 1981 OCTOBER 31

The Fiji Plateau is located between the New Hebrides and Tonga subduction zones and is characterized by a flat region of very deep and weak seismicity gently dipping to the west. The tectonic history of this region is very complex (e.g. Chase 1971), and no theory has yet been proposed which successfully explains the origin of the seismicity. The very few fault plane solutions obtained until now do not show any consistent pattern (Isacks & Molnar 1971). We applied the CMT method to seven events between 1977 and 1982, all of them with magnitude smaller than 5.5, and a CMT solution could be obtained for only two of them. The 1981 October 31 event has $m_b = 5.0$ and moment 7.7×10^{23}. The 1977 March 17 event, obtained with a very poor station coverage, has $m_b = 4.9$ and moment 8.1×10^{23}. Both fault plane mechanisms indicate east–west extension (nos 9 and 200 in Fig. 5), consistent with the solution no. 31 of Isacks & Molnar (1971).

On the identification of fault planes for deep earthquakes

Since its introduction (Dziewonski *et al.* 1981), the CMT method has proved very valuable for the quality of the solutions it provides. Here, we report some results of a recent study which relies on and independently proves the precision of the focal mechanisms derived from the CMT solutions. Giardini & Woodhouse (1983, 1984) analyse the seismicity of the deep Benioff zone in the Tonga Islands using 49 CMT solutions (Dziewonski & Woodhouse 1983; Dziewonski *et al.* 1983; this study) and a set of ~2200 hypocentres, taken from the ISC catalogue 1964–79 and relocated with the JHD technique (Douglas 1967; Dewey 1971). The purpose of the research is to test the hypothesis that plane shear is the principal mechanism responsible for deep seismicity. This is achieved by looking at the local seismicity surrounding each CMT solution from the direction of the null axis. In this way the nodal planes appear as straight lines which divide the focal sphere into quadrants and any lineation in the seismicity associated with a plane of failure becomes apparent and is parallel to a nodal plane.

The method has been notably successful in proving that deep events occur as ruptures on fault planes. Moreover, the Benioff zone, usually idealized as a continuous plane of seismicity, has emerged as a complex structure of shear bands which, through precise modes of deformation, release the general state of compression as episodes of shear instability. The lineations of seismicity are in good agreement with one, or sometimes both, of the fault planes for most of the analysed events, and group in precise families of seismicity characteristic of the different parts of the Benioff zone.

Fig. 13 shows some examples of the different patterns of seismicity. Each picture is centred on the CMT event. The hypocentral position and the seismic moment of the CMT event are indicated, together with the direction of view (azimuth and plunge angles). The lateral scale and the depth of the box in the direction of sight are also reported (in kilometres). Notice the very thin Benioff zone in Fig. 13(a), the breaking of the main seismic zone in Fig. 13(b), the complex three-planned structure with a conjugate plane in Fig. 13(c) and the mosaic of short parallel alignments in Fig. 13(d).

These structures are very sensitive to the direction from which they are viewed, namely the null axis. This indicates that the null axes are generally well constrained in the CMT

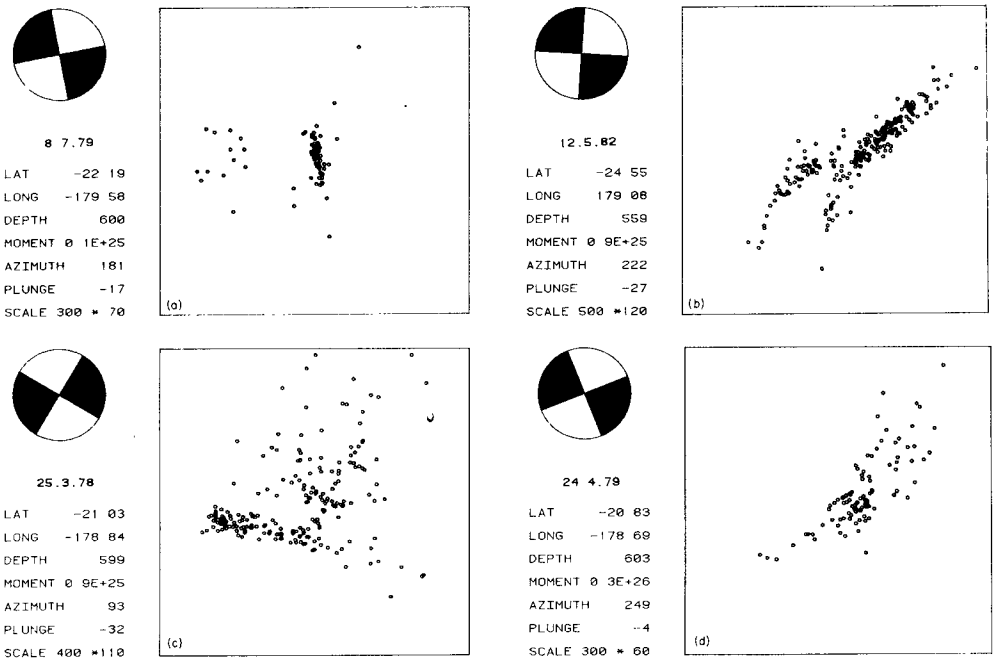

Figure 13. Each figure displays the seismicity centred on a particular CMT event and viewed from the direction of the null-axis of the CMT mechanism. All the four events are from the deepest part of the Benioff zone in the Tonga Islands region. Seismicity from the ISC catalogue (1964–79) relocated with the Joint Hypocentre Determination technique is shown. Hypocentral parameters, seismic moment and azimuth and plunge angles, defining the direction of the null-axis, are reported for each CMT solution. The scale indicates the lateral dimension and the depth of the box of seismicity used in each figure, both in kilometres. See explanations in the text for further details.

solutions. This, and the good parallelism between lineations of seismicity and nodal planes provide independent verification of the precision and reliability of the CMT method.

On the state of stress in the lithosphere

A dataset of precise and reliable fault plane solutions is the starting point of any study on the state of stress of subducting slabs. This has been one of the most debated and analysed subjects in the last 15 yr. The precise knowledge of the direction of maximum stress has been of primary importance, for example, in the analysis of the driving forces of convection and rheology of the subducting lithosphere (e.g. Richter 1979; Vassiliou 1983) and stress distribution connected with double seismic zones (e.g. Fujita & Kanamori 1981) and with bent or disrupted Benioff zones (e.g. Isacks & Molnar 1971). Maximum care has been used in these and many other studies in selecting reliable fault plane mechanisms. In fact, although a few thousands of fault plane solutions are now available, the quality of most of them is often not sufficient for high-precision studies. On the other hand, not enough moment tensor solutions, more reliable than first motion mechanisms, have been available until now.

We present here some examples from our dataset to show how the CMT method can provide the precise data needed for stress distribution analysis. Figs 14 and 15 show plots of the principal axes of the CMT solutions in a lower hemisphere equal-area projection, for a number of regions and for different source depths. Fig. 14(a) contains all the events in

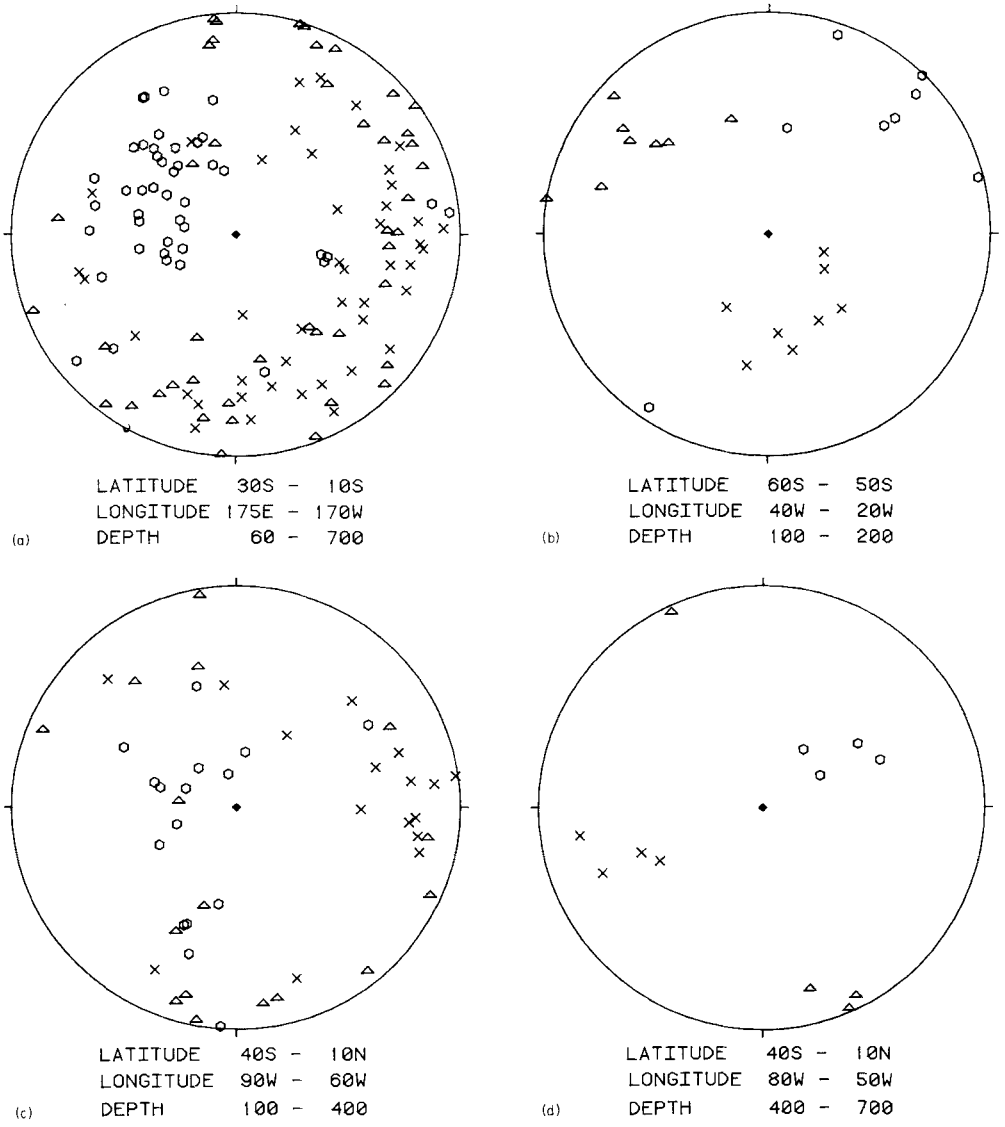

Figure 14. Each figure shows a projection of the principal axes of CMT mechanisms from selected regions and depths. The equal-area lower hemisphere projection of the focal sphere is used. Compression axes are indicated with ○, null axis with △ and tension axis with X; the small diamond indicates the centre in each figure. The selected Benioff zones are in Tonga Islands (a), Sandwich Islands (b), intermediate depth (c) and deep (d) South America.

the Tonga Islands region; the deviation from the double couple of these mechanisms has been plotted in Fig. 12(b). The characteristic state of down-dip compression of this slab, at all depths (Isacks & Molnar 1971), is confirmed by our results; a few anomalous solutions do not alter the general trend. The scatter in the compression axes, in this and in the following figures, is mainly due to the fact that we plot together events from parts of the slab having different strike and dip angles; nevertheless, this scatter is relatively small.

A precise study combining seismicity and moment tensor mechanisms has shown how in deep Tonga the local pattern of the compression axis varies from the general down-dip

direction, and how even anomalous solutions with down-dip tension or null axis can be explained in terms of the local stress distribution (Giardini & Woodhouse 1983, 1984). Notice also the apparently random distribution of the null and tension axes around the cluster of compression axes. This puzzling behaviour has been explained as typical of particular subregions of the Tonga Benioff zone characterized by in-plate subhorizontal motion acting as a mode of deformation of the slab in response to the general state of compression (Giardini & Woodhouse 1983, 1984).

Our results (Fig. 14a) show considerably less scatter than the fault plane solutions collected by Fujita & Kanamori (1981). They also indicate that the projection used by Vassiliou (1983) in a similar analysis is reliable only if a precise knowledge of the Benioff zone's geometry is available, and often this is not the case – not even for a well-studied region as the Tonga Arc (for example, compare the different interpretations of Billington 1980 and Giardini & Woodhouse, 1984).

Fig. 14(b) shows the CMT solutions in the Sandwich Arc subduction zone. In contrast to the Tonga Islands, this region shows no deep activity and strong down-dip extension at shallow and intermediate depths (see also Fig. 12a). Again, our solutions confirm, with less scatter, the results reported by Fujita & Kanamori (1981). Fig. 14(c, d) shows all the events in South America. Here the slab is characterized by a general state of down-dip tension at intermediate depths (Fig. 14c), and steeper down-dip compression in the deeper part (Fig. 14d); our results fully confirm this typical stress pattern.

Fig. 15(a, b) shows solutions for the intermediate depth events in the Banda Sea and New Hebrides regions. Both are dominated by down-dip extension at these depths; noteworthy, however, are the two events showing down-dip compression in the deeper part of the New Hebrides slab.

Fig. 15(c, d) reports deep events in Japan and the Philippine Benioff zones. The Japanese events exhibit very shallow down-dip compression and large lateral scatter of the compression axis in the plane of the slab. This was noted by Fujita & Kanamori (1981) for intermediate depth events in the same region and led them to speak of 'in-plate' instead of 'down-dip' axes. We find this lateral scatter only in Japan, with a few solutions, and perhaps in South America, and we prefer therefore to maintain the terminology 'down-dip' as used by Isacks & Molnar (1971).

We would like to mention that our solutions confirm the results of many regional studies. We have limited ourselves here to a comparison with a systematic analysis which collected the best fault plane mechanisms available for intermediate depth events (Fujita & Kanamori 1981). The fact that our results show systematically less scatter than theirs is an indication of the uniformity and precision of the CMT solutions.

Conclusions

(1) GDSN and IDA have provided high quality digital data since 1977. In particular, the exceptional dynamic range of the SRO/ASRO instruments allows us to invert for moment tensors in the range between 7×10^{23} and 1.4×10^{28} using the same algorithm.

(2) Owing to its characteristics of precision, rapidity and objectivity, the CMT method is the most suitable technique available at present for systematic processing of large numbers of earthquakes. More than half of the moment tensor solutions available for deep events are obtained and presented in this study.

(3) Among the centroid parameters, the epicentral position is the less reliable, because of the bias due to the lateral heterogeneity of the Earth. CMT depths appear to be more reliable than catalogue depths, owing to the inclusions of all the depth phases in the inversion.

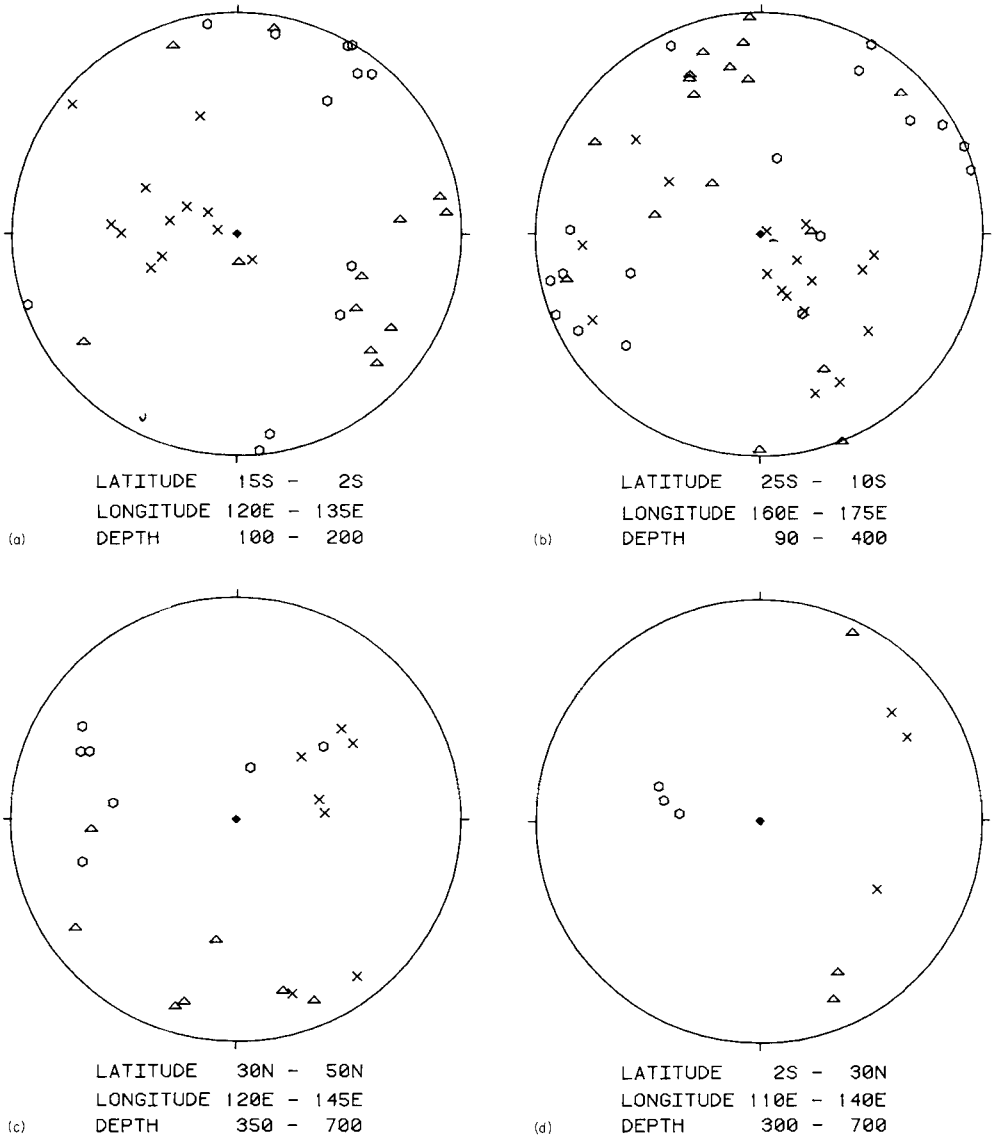

Figure 15. Same as Fig. 14 but for events from the shallower part of the Banda Sea subduction zone (a), the New Hebrides Islands region (b), and the deeper part of the Benioff zones in Japan (c) and Philippine Islands (d) regions.

(4) The shift in origin time is proportional to the cube root of the seismic moment, in agreement with the relation proposed by Kanamori & Anderson (1975). The large time shift of deep events is a strong indication that deep earthquakes consist of multiple shocks.

(5) The body-wave magnitude scale m_b shows large scatter with respect to the seismic moment; for every value of m_b the moments typically range over two orders of magnitude. Therefore, maximum care should be used in studies of seismicity based on the magnitude scale m_b. Although affected by a larger scatter, however, m_b seems to serve as well as the broad-band body-wave magnitude m_B in quantifying deep earthquakes, at least for events smaller than 5×10^{26}.

(6) The deviation from the double couple seems to decrease with increasing seismic moment. Correlations have emerged between the sign of the deviation and the state of stress of the subducting slabs. CMT mechanisms showing down-dip compression are also dominated by the eigenvalue associated with the compression axis; regions of down-dip tension show mechanisms dominated by the tensional eigenvalue.

(7) Comparison of CMT solutions with moment tensors published by other authors show good agreement among mechanisms obtained using different techniques and different sources of waveform data, confirming the moment tensor representation as the more precise way of characterizing the size and geometry of the seismic source.

(8) The precise solutions provided by the CMT method have been indispensable in a study of deep seismicity which, by correlating patterns of hypocentre distribution with the nodal planes, has shown that deep seismicity is due to shear failure on fault planes and has provided new indications of the mechanical behaviour of subducting slabs.

(9) Comparison with precise published focal mechanisms shows the CMT method to be very suitable for analysis of the state of stress in subduction zones. Our results confirm the patterns of down-dip allignment of the compression or tension axes identified by Isacks & Molnar (1971).

Acknowledgments

The CMT technique has been developed and implemented by Professors A. M. Dziewonski and J. H. Woodhouse. I would like to express to them my gratitude for the encouragement, help and assistance they provided during my use of the CMT method. I also thank them for numerous discussions of the material and for critically reviewing the manuscript, and I acknowledge the free use I have made of a number of computer programs. I am grateful to Professor E. Boschi for his encouragement during my study.

This research was supported by the National Science Foundation grants EAR82-13330 and EAR80-26441.

References

Abe, K., 1982. Magnitude, seismic moment and apparent stress for major deep earthquakes, *J. Phys. Earth*, **30**, 321–330.

Abe, K. & Kanamori, H., 1979. Temporal variation of the activity of intermediate and deep focus earthquakes, *J. geophys. Res.*, **84**, 3589–3595.

Agnew, D., Berger, J., Buland, R., Farrell, W. & Gilbert, F., 1976. International Deployment of Accelerometers: a network of very long period seismology, *Eos, Trans. Am. geophys. Un.*, **57**, 180–188.

Aki, K. & Richards, P. G., 1980. *Quantitative Seismology*, **1**, H. W. Freeman, San Francisco, 557 pp.

Backus, G. E., 1977. Interpreting the seismic glut moments of total degree of two or less, *Geophys. J. R. astr. Soc.*, **51**, 1–25.

Billington, S., 1980. The morphology and tectonics of the subducted lithosphere in the Tonga–Fiji–Kermadec region from seismicity and focal mechanism solutions, *PhD thesis*, Cornell University.

Billington, S. & Isacks, B. L., 1975. Identification of fault planes associated with deep earthquakes, *Geophys. Res. Lett.*, **2**, 63–66.

Billington, S., Isacks, B. L. & Barazangi, M., 1977. Spatial distribution and focal mechanisms of mantle earthquakes in the Hindu Kush–Pamir region: a contorted Benioff zone, *Geology*, **5**, 699–704.

Chase, C. G., 1971. Tectonic history of the Fiji Plateau, *Bull. geol. Soc. Am.*, **82**, 3087–3110.

Chung, W. Y. & Kanamori, H., 1980. Variation of seismic source parameters and stress drops within a descending slab and its implications in plate mechanics, *Phys. Earth planet. Int.*, **23**, 134–159.

Dewey, J. W., 1971. Seismicity studies with the method of joint hypocenter determination, *PhD thesis*, University of California at Berkeley.

Douglas, A., 1967. Joint epicenter determination, *Nature*, **215**, 47–48.

Dziewonski, A. M. & Anderson, D. L., 1981. Preliminary Reference Earth Model (PREM), *Phys. Earth planet. Int.*, **25**, 297–356.

Dziewonski, A. M., Chou, T. A. & Woodhouse, J. H., 1981. Determination of earthquake source parameters from waveform data for studies of global and regional seismicity, *J. geophys. Res.*, **86**, 2825–2852.

Dziewonski, A. N., Friedman, A., Giardini, D. & Woodhouse, J. H., 1983. Centroid-Moment Tensor solutions for 308 moderate and large earthquakes of 1982, *Phys. Earth planet. Int.*, **33**, 76–90.

Dziewonski, A. M. & Woodhouse, J. H., 1983. An experiment in systematic study of global seismicity: centroid–moment tensor solutions for 201 moderate and large earthquakes of 1981, *J. geophys. Res.*, **88**, 3247–3271.

Ekström, G. & Dziewonski, A. M., 1983. Moment tensor solutions of Mammoth Lake earthquakes, (abstract), *Eos, Trans. Am. geophys. Un.*, **64**, 262.

Fujita, K. & Kanamori, H., 1981. Double seismic zones and stresses of intermediate depth earthquakes, *Geophys. J. R. astr. Soc.*, **66**, 131–156.

Fukao, Y., 1972. Source process of a large deep-focus earthquake and its tectonic implications – the western Brazil earthquake of 1963, *Phys. Earth planet. Int.*, **5**, 61–76.

Furumoto, M. & Nakanishi, I., 1983. Source times and scaling relations of large earthquakes, *J. geophys. Res.*, **88**, 2191–2198.

Giardini, D., 1983. Regional deviation of earthquake source mechanisms from the "double-couple" model, *Proc. Enrico Fermi int. Sch. Phys.*, **85**, eds Kanamori, H. & Boschi, E., North-Holland, Amsterdam, in press.

Giardini, D. & Woodhouse, J. H., 1983. Deformation within the Tonga subduction zone (abstract), *Eos, Trans. Am. geophys. Un.*, **64**, 264.

Giardini, D. & Woodhouse, J. H., 1984. Deep seismicity and modes of deformation in the Tonga subduction zone, *Nature*, in press.

Gilbert, F., 1981. An introduction to low-frequency seismology, in *Proc. Enrico Fermi Int. Sch. Phys.*, **78**, 41–81, eds Dziewonski, A. M. & Boschi, E., North-Holland, Amsterdam.

Gutenberg, B., 1945. Magnitude determination for deep-focus earthquakes, *Bull. seism. Soc. Am.*, **35**, 117–130.

Gutenberg, B. & Richter, C. F., 1956. Magnitude and energy of earthquakes, *Annali Geofis.*, **9**, 1–15.

Hartzell, S., 1979. Analysis of the Bucharest strong ground motion record from the March 4, 1977, Romanian earthquake, *Bull. seism. Soc. Am.*, **69**, 513–530.

Isacks, B. & Molnar, P., 1971. Distribution of stresses in the descending lithosphere from a global survey of focal mechanism solutions of mantle earthquakes, *Rev. geophys. Space. Phys.*, **9**, 103–174.

Kanamori, H., 1983. Magnitude scale and quantification of earthquakes, *Tectonophys.*, **93**, 185–199.

Kanamori, H. & Anderson, D. L., 1975. Theoretical basis of some empirical relations in seismology, *Bull. seism. Soc. Am.*, **65**, 1073–1095.

Kanamori, H. & Given, J. W., 1981. Use of long-period surface waves for fast determination of earthquake source parameters, *Phys. Earth planet. Int.*, **27**, 8–31.

Kanamori, H. & Given, J. W., 1982. Use of long period surface waves for rapid determination of earthquake source parameters, 2. Preliminary determination of source mechanism of large earthquakes ($M_S \geqslant 6.5$) in 1980, *Phys. Earth planet. Int.*, **30**, 260–268.

Knopoff, L. & Randall, M. J., 1970. The compensated linear-vector dipole, *J. geophys. Res.*, **75**, 4957–4963.

Malgrange, M. & Okal, E. A., 1983. Seismological investigations of a large slab-tearing event (abstract), *Eos, Trans. Am. geophys. Un.*, **64**, 262.

Masters, G. & Gilbert, F., 1979. Source retrieval from a sparse long period network (abstract), *Eos, Trans. Am. geophys. Un.*, **60**, 879.

Mueller, G., Bonjer, K. P., Stockl, H. & Enescu, D., 1978. The Romanian earthquake of March 4, 1977, I: Rupture process inferred from fault-plane solution and multiple event analysis, *J. Geophys.*, **44**, 203–218.

Noguchi, S. & Abe, K., 1977. Earthquakes source mechanism and M_s–m_b relation, *Zisin II*, **30**, 487–507 (in Japanese, with English abstract).

Peterson, J., Butler, H. M., Holcomb, L. G. & Hutt, C. R., 1976. The Seismic Research Observatory, *Bull. seism. Soc. Am.*, **66**, 2049–2068.

Richter, F. M., 1979. Focal mechanisms and seismic energy release of deep and intermediate earthquakes in the Tonga–Kermadec region and their bearing on the depth extent of mantle flow, *J. geophys. Res.*, **84**, 6783–6795.

Sasatani, T., 1976. Mechanism of mantle earthquakes near the junction of the Kurile and northern Honshu arcs, *J. Phys. Earth*, **24**, 341–354.

Silver, P. G. & Jordan, T. H., 1982. Optimal estimation of scalar seismic moment, *Geophys. J. R. astr. Soc.*, **70**, 755–787.

Silver, P. G. & Jordan, T. H., 1983. Total-moment spectra of fourteen large earthquakes, *J. geophys. Res.*, **88**, 3273–3293.

Sipkin, S. A., 1982. Estimation of earthquake source parameters by the inversion of waveform data: synthetic seismograms, *Phys. Earth planet. Int.*, **30**, 242–259.

Talandier, J. & Okal, E. A., 1979. Human perception of *T* waves: the June 22, 1977 Tonga Earthquake felt on Tahiti, *Bull. seism. Soc. Am.*, **69**, 1475–1486.

Vassiliou, M. S., 1983. The energy release in earthquakes and Subduction zone seismicity and stress in slabs, *PhD thesis*, California Institute of Technology.

Vassiliou, M. S. & Kanamori, H., 1982. The energy release in earthquakes, *Bull. seism. Soc. Am.*, **72**, 371–387.

Woodhouse, J. H., 1981. The calculation of the complete normal-mode spectrum of the earth using finite difference methods, *Semiannual Techn. Rep, Seismic Discrimination, 1 October 1980–31 March 1981*, pp. 73–76. Lincoln Laboratory, Massachusetts Institute of Technology, Cambridge.

Wyss, M. & Molnar, P., 1972. Source parameters of intermediate and deep focus earthquakes in the Tonga Arc, *Phys. Earth planet. Int.*, **6**, 279–292.